# Just a Proton: Distinguishing the Two Electronic States of Five-Coordinate High-Spin Iron(II) Porphyrinates with Imidazole/ate Coordination

Chuanjiang Hu,[†,‡] Corinne D. Sulok,[§] Florian Paulat,[§] Nicolai Lehnert,*[,§]
Anna I. Twigg,[||] Michael P. Hendrich,*[,||] Charles E. Schulz,*[,⊥] and
W. Robert Scheidt*[,†]

*The Department of Chemistry and Biochemistry, University of Notre Dame, Notre Dame,
Indiana 46556, Department of Chemistry, University of Michigan, 930 North University Avenue,
Ann Arbor, Michigan 48109, Department of Chemistry, Carnegie Mellon University,
4400 Fifth Avenue, Pittsburgh, Pennsylvania 15213, and Department of Physics, Knox College,
Galesburg, Illinois 61401*

Received September 7, 2009; E-mail: scheidt.1@nd.edu; lehnertn@umich.edu;
hendrich@andrew.cmu.edu; cschulz@knox.edu

**Abstract:** We report detailed studies on two $S = 2$ electronic states of high-spin iron(II) porphyrinates. These two states are exemplified by the five-coordinate derivatives with either neutral imidazole or anionic imidazolate as the axial ligand. The application of several physical methods all demonstrate distinctive differences between the two states. These include characteristic molecular structure differences, Mössbauer spectra, magnetic circular dichroism spectroscopy, and integer-spin EPR spectral distinctions. These distinctions are supported by DFT calculations. The two states are characterized by very different spatial properties of the doubly occupied orbital of the high-spin that are consonant with the physical properties.

## Introduction

The wide range of physiological functions carried out by the heme proteins with the same prosthetic group, the iron derivative of protoporphyrin IX, has continued to fascinate and perplex. Some aspects of heme protein function appear to be controlled by obvious changes in the proximal axial ligand to iron. For example, the cytochrome P-450 monooxygenases and NO synthase (NOS) are coordinated by an anionic cysteine ligand and the catalases are coordinated by an anionic tyrosinate. However, the most common proximal ligand in the heme proteins is the histidyl residue that is equivalent to imidazole, a nominally neutral ligand. Proteins with histidine ligation still maintain a wide variety of functions that include oxygen transport and storage in the globins, oxygen respiration in cytochrome *c* oxidase and oxygen utilization and oxidation in the peroxidases, oxidases, cyclooxygenase, NO reduction in bacterial NO reductase (NorBC), NO signaling in soluble guanylate cyclase (sGC), and NO transport in nitrophorins.

A common feature in many of these systems is the appearance of a hydrogen bond to the proximal histidine ligand as shown in Figure 1 for deoxymyoglobin[1] and horseradish peroxidase.[2] The strength of these hydrogen bonds is thought to vary from very weak proton donation to complete donation to form the
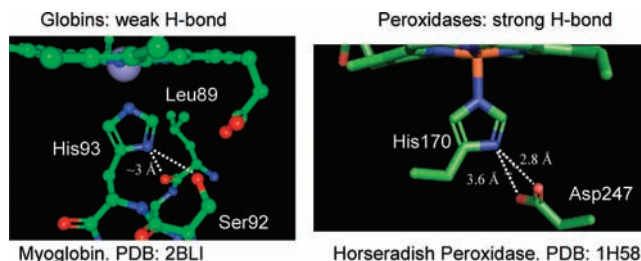


**Figure 1.** Comparison of the hydrogen bonding network involving the proximal histidine in heme proteins. Left: myoglobin (Mb) as an example for the case of weak hydrogen bonding. Right: horseradish peroxidase (HRP) constitutes the case of strong hydrogen bonding.

imidazolate ligand.[3−9] The notion that a strong hydrogen bond has a strong influence on heme protein behavior is longstanding but has been difficult to investigate in a systematic manner. Clearly there are significant differences in the nature of the hydrogen bonds formed to the proximal histidine in different

[†] University of Notre Dame.
[‡] Present address: College of Chemistry, Chemical Engineering and Materials Science, Soochow University, Suzhou 215123 China.
[§] University of Michigan.
[||] Carnegie Mellon University.
[⊥] Knox College.

(1) Vojtechovsky, J.; Chu, K.; Berendzen, J.; Sweet, R. M.; Schlichting, I. *Biophys. J.* **1999**, *77*, 2153.
(2) Berglund, G. I.; Carlsson, G. H.; Smith, A. T.; Szöke, H.; Henriksen, A.; Hajdu, J. *Nature* **2002**, *417*, 463.
(3) Peisach, J.; Blumberg, W. E.; Adler, A. *Ann. N.Y. Acad. Sci.* **1973**, *206*, 310.
(4) Nicholls, P. *Biochim. Biophys. Acta* **1962**, *60*, 217.
(5) Mincey, T.; Traylor, T. G. *J. Am. Chem. Soc.* **1979**, *101*, 765.
(6) Teroaka, J.; Kitagawa, T. *Biochem. Biophys. Res. Commun.* **1980**, *93*, 674.
(7) Morrison, M.; Schonbaum, G. R. *Annu. Rev. Biochem.* **1976**, *45*, 861.
(8) Peisach, J. *Ann. N.Y. Acad. Sci.* **1975**, *244*, 187.
(9) Valentine, J. S.; Sheridan, R. P.; Allen, L. C.; Kahn, P. *Proc. Natl. Acad. Sci. U.S.A.* **1979**, *76*, 1009.
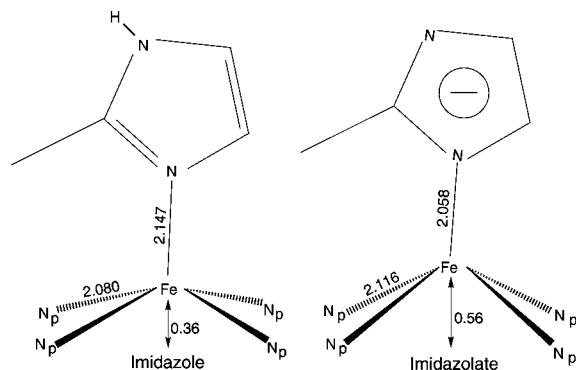
**Figure 2.** Comparison of the coordination group geometries (averaged values) of the high-spin iron(II) porphyrinates with 2-methylimidazole (left) and 2-methylimidazolate (right) as the axial ligand.

heme proteins. Three distinctly different types of hydrogen bonds are formed: the globins and a number of other proteins form a weak hydrogen bond between histidine and a nearby carbonyl or alcohol group, the peroxidases that are hydrogen-bonded to a conserved aspartate and the oxidases that are hydrogen-bonded to a conserved glutamate. The idea continues to appeal that in the peroxidases, which have a conserved aspartate that is hydrogen-bonded to the histidine, the histidine shows imidazolate-like character. This strong hydrogen bond is thought to stabilize higher oxidation states of iron and to distinctly alter the chemical behavior of the peroxidases relative to the globins. Nevertheless, the role of this hydrogen bond is still one of the unresolved issues concerning the peroxidases.

As part of a systematic study of five-coordinate iron(II), we have synthesized and characterized a number of five-coordinate imidazole- and imidazol*ate*-ligated iron(II) porphyrinate derivatives.[10−15] This work reports the effects observed on the molecular and electronic structure when an imidazole ligand in five-coordinate iron(II) porphyrinate derivatives of the type [Fe(Por)(2-MeHIm)][16] is deprotonated.[12] Both imidazole- and imidazolate-ligated iron(II) porphyrinates exhibit an $S = 2$ (quintet) ground state, but the structural parameters of the coordination group are distinct with both axial and equatorial bond distance differences and large differences in the displacement of iron from the porphyrin plane. These differences are schematically depicted in Figure 2 for the iron(II) derivatives with imidazole and imidazol*ate* as the axial ligand and where averaged values for several examples of each have been given.

In addition to the structural differences, characterization by Mössbauer spectroscopy showed that the imidazole derivatives

were electronically quite distinct from the imidazolate complexes. Measurements in applied magnetic field allowed the determination of the sign of the quadrupole splitting that was found to be negative for all imidazole derivatives ($V_{zz} < 0$) and positive ($V_{zz} > 0$) for the imidazolate species. Moreover, the asymmetry parameter for the imidazole species was found to be very large, whereas that for the imidazolate derivatives was small. The differences in the Mössbauer spectra obtained in applied magnetic fields indicate that the doubly occupied d orbital is different in the two classes. This change in the d-electron configuration is clearly consistent with all observed differing features of the two classes. These results are strikingly similar to those observed for protein examples. Reduced HRP was studied by Mössbauer spectroscopy and compared with deoxymyoglobin.[17,18] These Mössbauer studies, in a strong magnetic field, showed remarkable differences between reduced HRP and deoxymyoglobin even though both are five-coordinate hemes with histidine as the axial ligand. Reduced HRP has a positive quadrupole splitting constant and a rather small asymmetry value,[18] whereas deoxyMb has a negative value of the quadrupole splitting constant and a large asymmetry constant.[19] To our knowledge, these Mössbauer measurements in applied magnetic field are the only ones available for iron(II) heme proteins with a proximal histidine, although deoxymyoglobin and deoxyhemoglobin have been often measured.

These results led us to conclude that there are at least two $S = 2$ states of high-spin iron(II) porphyrinates with distinctly different d-electron configurations that arise from proximal ligand effects. The one class of high-spin iron(II) derivatives, which we will call Class **N**, is represented by the coordination of neutral nitrogen donors in small molecule systems and in the proteins by deoxymyoglobin and deoxyhemoglobin. The second class, which we will call Class **A**, is represented by the coordination of anionic imidazolate and other anions in small molecule systems and reduced HRP in the proteins. The important class of cysteine-ligated hemes and heme proteins also probably belong to this class although this has been established only for heme derivatives.[20] In this paper, we explore a number of characterization processes that could provide ways to distinguish between the two classes. These include integer-spin EPR measurements, magnetic circular dichroism spectroscopy, structure, and a reexamination of the Mössbauer fitting analysis of spectra in applied magnetic field. We have also explored DFT calculations and how different functionals replicate (or fail to) the experimental results. We conclude that the distinction of Class **N** and Class **A** electronic structures represents a real and useful dichotomy for high-spin iron(II) porphyrinates. We further conclude that all methods tested allow

(10) Ellison, M. K.; Schulz, C. E.; Scheidt, W. R. *Inorg. Chem.* **2002**, *41*, 2173.

(11) Hu, C.; Roth, A.; Ellison, M. K.; An, J.; Ellis, C. M.; Schulz, C. E.; Scheidt, W. R. *J. Am. Chem. Soc.* **2005**, *127*, 5675.

(12) Hu, C.; Noll, B. C.; Schulz, C. E.; Scheidt, W. R. *J. Am. Chem. Soc.* **2005**, *127*, 15018.

(13) Hu, C.; An, J.; Noll, B. C.; Schulz, C. E.; Scheidt, W. R. *Inorg. Chem.* **2006**, *45*, 4177.

(14) Hu, C.; Noll, B. C.; Piccoli, P. M. B.; Schultz, A. J.; Schulz, C. E.; Scheidt, W. R. *J. Am. Chem. Soc.* **2008**, *130*, 3127.

(15) Hu, C.; Noll, B. C.; Schulz, C. E.; Scheidt, W. R. *Inorg. Chem.* **2008**, *47*, 8884.

(16) The following abbreviations are used in this paper: MCD, magnetic circular dichroism; EPR, electron paramagnetic resonance; SOC, spin-orbit coupling; Por, generalized porphyrin dianion; OEP, dianion of octaethylporphyrin; TPP, dianion of *meso*-tetraphenylporphyrin; TpivPP, dianion of picket fence porphyrin; 2-MeHIm, 2-methylimidazole; 2-MeIm⁻; 2-methylimidazolate: 5C, five-coordinate; hs, high-spin; HRP, horseradish peroxidase; CuEDTA, copper salt of ethylenedi-aminetetraacetic acid; 222 or kryptofix-222, 4,7,13,16,21,24-hexa-oxo-1,10-diazabicyclo[8.8.8]hexacosane; $N_p$, porphyrinato nitrogen.

(17) Debrunner, P. In *Iron Porphyrins Part 3*; Lever, A. B. P., Gray, H. B., Eds.; VCH Publishers Inc.; New York, 1983; Chapter 2.

(18) Champion, P. M.; Chiang, R.; Münck, E.; Debrunner, P.; Hager, L. P. *Biochemistry* **1975**, *14*, 4159.

(19) Kent, T. A.; Spartalian, K.; Lang, G.; Yonetani, T.; Reed, C. A.; Collman, J. P. *Biochem. Biophys. Acta* **1979**, *580*, 245.

(20) The position of the iron(II) thiolato complexes is somewhat ambiguous. Their structural parameters are closer to those of Class **N**, whereas their Mössbauer properties have positive values of the quadrupole splitting constant consistent with Class **A** species.[21]

(21) Schappacher, M.; Ricard, L.; Weiss, R. R.; Montiel-Montoya, R.; Bill, E.; Trautwein, A. X. *Inorg. Chem.* **1989**, *28*, 4639.

for the detection of electronic state distinctions (or differences) and that they are applicable to a variety of systems.

## Experimental Section

**General Information.** All reactions and manipulations for the iron(II) porphyrinate derivatives were carried out under argon using a double-manifold vacuum line, Schlenkware and cannula techniques. Benzene and hexanes were distilled over sodium benzophenone ketyl. Chlorobenzene was washed with concentrated sulfuric acid, then with water until the aqueous layer was neutral, dried with $MgSO_4$, and distilled twice over $P_2O_5$ under argon. Hexanes were distilled over sodium benzophenone. All solvents were degassed prior to use by three freeze/pump/thaw cycles. Ethanethiol (Aldrich) was used as received. 2-Methylimidazole (Aldrich) was recrystallized from toluene/methanol and dried under vacuum. All other chemicals were used as received from Aldrich or Fisher. *meso*-Tetraphenylporphyrin ($H_2$TPP) was prepared according to Adler et al.[22] and octaethylporphyrin ($H_2$OEP) was purchased from Midcentury. [Fe(Por)Cl] derivatives were prepared according to a modified Adler preparation[23] and used to prepare the analogous [Fe(Por)]$_2$O species.[24]

**Synthesis of [K(2-MeIm⁻)].** In the drybox, 2-methylimidazole (1.52 g, 19 mmol) was dissolved in 20 mL of THF, then KH (0.72 g, 18 mmol) was added slowly. The mixture was stirred for 3 h, then filtered by cannula, the resulting solid was dried under vacuum at 60 °C for 6 h, collected, and stored under argon.

**Synthesis of [Fe(Por)] Derivatives.** [Fe(Por)]$_2$O (0.03 mmol) was dissolved in 10 mL of benzene, and 1 mL of ethanethiol was added by syringe. The mixture was stirred at room temperature for 3 days, then was layered with hexanes for crystallization. Crystalline [Fe(Por)] was collected after several days, stored under argon and used for preparing solutions for the MCD measurements.

**Synthesis of [K(222)][Fe(OEP)(2-MeIm⁻)].** [Fe(OEP)]$_2$O (38 mg, 0.03 mmol) was dissolved in 10 mL of benzene, 1 mL of ethanethiol was added by syringe, and stirred at room temperature for 3 days. The solvent was removed under vacuum and the solid was dried for another hour. A suspension of excess K(2-MeIm⁻) (28 mg, 0.23 mmol) and Kryptofix 222[16] (70 mg, 0.19 mmol) in 15 mL of chlorobenzene was added to the [Fe(II)(OEP)] solid by cannula, then stirred for 1/2 h and cannula filtered to another Schlenk flask. X-ray quality crystals were obtained after three weeks by liquid diffusion using hexanes as nonsolvent in 8 mm × 250 mm sealed glass tubes.

**Synthesis of [K(222)][Fe(TPP)(2-MeIm⁻)].** [Fe(TPP)]$_2$O (40 mg, 0.03 mmol) was dissolved in 10 mL of benzene, 1 mL of ethanethiol was added by syringe, and stirred at room temperature for 3 days. The solvent was removed under vacuum, the solid was dried for another hour, and then dissolved in 10 mL of toluene. A suspension of excess K(2-MeIm⁻) (24 mg, 0.20 mmol) and Kryptofix 222 (49 mg, 0.13 mmol) in 10 mL of toluene was added to the above solution, the resulting precipitate was cannula filtered, dried under vacuum for 1/2 h, then dissolved in 10 mL of chlorobenzene. The resulting solution was cannula filtered to another Schlenk flask. X-ray quality crystals were obtained after three weeks by liquid diffusion using hexanes as nonsolvent in 8 mm × 250 mm sealed glass tubes.

**Synthesis of [Na(222)][Fe(TPP)Cl].** Crystals of Na(222)-[Fe(TPP)Cl] were initially prepared accidentally during the reaction of [Fe(TPP)] with $NaN_3$ in $CH_2Cl_2$. [Fe(TPP)]$_2$O (40 mg, 0.03 mmol) was dissolved in 10 mL of chlorobenzene, and 1 mL of

ethanethiol was added by syringe. The mixture was stirred at room temperature for 3 days, then the solution was transferred into a Schlenk flask containing sodium azide (5 mg) and Kryptofix 222 (27 mg, 0.07 mmol). The mixture was stirred for 1 h, the resulting precipitate was filtered and dried under vacuum for 0.5 h. Then it was redissolved in $CH_2Cl_2$ (6 mL), and filtered. X-ray quality crystals were obtained in 8 mm × 250 mm sealed glass tubes by liquid diffusion using hexanes as nonsolvent. There were several different crystals formed, one of which was Na(222)[Fe(TPP)Cl], whose structure is described herein.

**Instrumental Techniques.** Mössbauer measurements were performed on a constant acceleration spectrometer from 4.2 to 298 K in small field and at 4.2 K in several fields between 0.75 and 9 T using a superconducting magnet system (Knox College). Microcrystalline solids for Mössbauer measurements were obtained by liquid diffusion in Schlenk tubes using hexanes as the nonsolvent. The solids were isolated in an inert-atmosphere box and immobilized in Apiezon M grease.

MCD spectra were obtained on frozen glasses in the mixed solvent of toluene and methylene chloride (1:1) at liquid He temperatures (1.8−25 K). A CD spectropolarimeter (Jasco 810) with S1 and S20 photomultiplier tubes as detectors were used where the sample compartment was modified to accommodate an Oxford instruments SM4−7T magnetocryostat. Spectral sample solutions were prepared from Fe(TPP) in the presence of excess ligand (and 222 for the anionic derivatives) and concentrations were determined by UV−vis spectroscopy at the same time as the MCD measurements. The samples were frozen in metallic sample compartments between 2 Infrasil quartz disks separated by 3 mm neoprene spacers. Typical sample concentrations were in the range of 0.2−1.0 mM (University of Michigan).

X-band EPR spectra of powder and solution samples were recorded on a Bruker 300 spectrometer equipped with an Oxford ESR-910 liquid helium cryostat and a Bruker bimodal cavity for generation of the microwave fields parallel and perpendicular to the static field. The microwave frequency was calibrated with a frequency counter, and the magnetic field was calibrated with a NMR gaussmeter. The sample temperature was calibrated with a carbon-glass resistor (Lake Shore CGR-1−1000) placed in an EPR tube to mimic a sample. The powder samples were prepared in EPR tubes fitted with graded quartz to Pyrex tops and flame-sealed. The solution samples were 5−6 mM in chlorobenzene and frozen in standard quartz tubes. All experimental data were collected under nonsaturating microwave conditions with a modulation frequency of 100 kHz. The EPR spectra and temperature dependence were analyzed by diagonalization of the spin Hamiltonian $H = S \cdot D \cdot S + \beta S \cdot g \cdot B$. The simulations were generated with consideration of all intensity factors relative to a CuEDTA spin standard which allowed computation of simulated spectra for a specific sample amount. The simulations therefore allow a quantitative determination of signal intensities. The Windows software package (Spin-Count) is available for general application (www.chem.cmu.edu/groups/hendrich/facilities/index.html) (Carnegie Mellon University).

**DFT Calculations.** The structures of the complexes [Fe(TPP)(2-MeHIm)], [Fe(TPP)(2-MeIm⁻)]⁻, and [Fe(TPP)Cl]⁻ were fully optimized without simplifications applying the BP86 functional[25] together with Ahlrichs' TZVP basis set[26] using Gaussian 03.[27] Zero-field splitting and Mössbauer parameters were calculated for both the DFT-optimized and crystal structures (with hydrogen atoms added in idealized positions) using the program ORCA.[28] These

---

(22) Adler, A. D.; Longo, F. R.; Finarelli, J. D.; Goldmacher, J.; Assour, J.; Korsakoff, L. *J. Org. Chem.* **1967**, *32*, 476.

(23) (a) Adler, A. D.; Longo, F. R.; Kampus, F.; Kim, J. *J. Inorg. Nucl. Chem.* **1970**, *32*, 2443. (b) Buchler, J. W. In *Porphyrins and Metalloporphyrins*; Smith, K. M., Ed.; Elsevier Scientific Publishing: Amsterdam, The Netherlands, 1975; Chapter 5.

(24) (a) Fleischer, E. B.; Srivastava, T. S. *J. Am. Chem. Soc.* **1969**, *91*, 2403. (b) Hoffman, A. B.; Collins, D. M.; Day, V. W.; Fleischer, E. B.; Srivastava, T. S.; Hoard, J. L. *J. Am. Chem. Soc.* **1972**, *94*, 3620.

(25) (a) Becke, A. D. *Phys. Rev. A* **1988**, *38*, 3098. (b) Perdew, J. P. *Phys. Rev. B* **1986**, *33*, 8822.

(26) (a) Schaefer, A.; Horn, H.; Ahlrichs, R. *J. Chem. Phys.* **1992**, *97*, 2571. (b) Schaefer, A.; Huber, C.; Ahlrichs, R. *J. Chem. Phys.* **1994**, *100*, 5829.

(27) Frisch, M. J.; et al. *Gaussian 03*; Gaussian, Inc: Pittsburgh, PA, 2003.

(28) Neese, F. *ORCA - an ab initio, density functional and semiempirical program package*, version 2.6 rev 40; University of Bonn: Bonn, Germany, 2007.
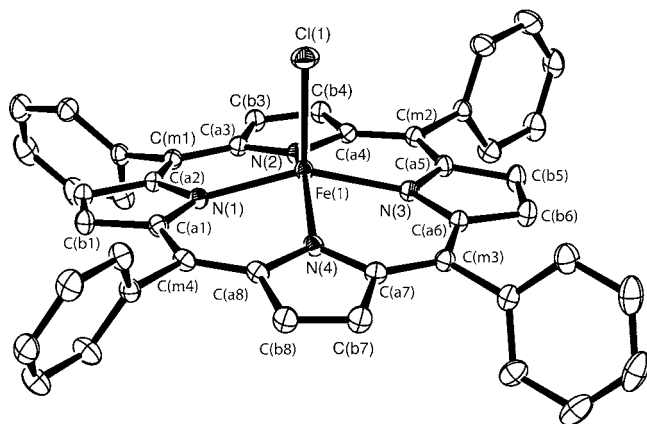
**Figure 3.** ORTEP diagram (50% probability ellipsoid) of the [Fe(TPP)Cl]⁻ anion illustrating the atom labeling scheme. Hydrogen atoms have been omitted for clarity.

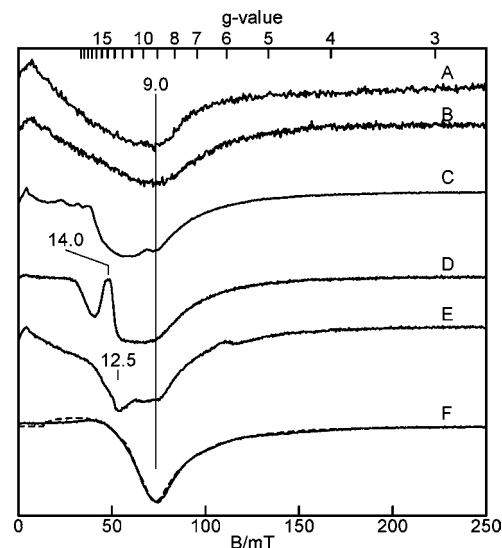**Table 1.** Selected Distances (Å) for Iron(II) Porphyrinates with Anionic Ligands

| complex | ⟨Fe−N$_p$⟩$^{a,b}$ | Fe−L$^b$ | ΔN$_4{}^b$ | ref |
|---|---|---|---|---|
| [Fe(TPP)Cl]⁻ | 2.1161(11) | 2.3400(5) | 0.56 | tw$^d$ |
| [Fe(TpivPP)Cl]⁻ | 2.108(15) | 2.301(2) | 0.53 | 32 |
| [Fe(TPP)(2-MeIm⁻)]⁻ | 2.118(13) | 2.056(81)$^c$ | 0.56 | 12 |
| [Fe(OEP)(2-MeIm⁻)]⁻ | 2.113(4) | 2.060(2) | 0.56 | 12 |
| [Fe(TpivPP)(2-MeIm⁻)]⁻ | 2.11(2) | 2.002(15) | 0.52 | 33 |
| [Fe(TpivPP)(NO₃)]⁻ | 2.070(16) | 2.069(4) | 0.42 | 34 |
| [Fe(TPP)(SC₂H₅)]⁻ | 2.096(4) | 2.360(2) | 0.52 | 35 |
| [Fe(TpivPP)(SC₂H₅)]⁻ | 2.074(10) | 2.324(2) | 0.44 | 21 |
| [Fe(TpivPP)(OC₆H₅)]⁻ | 2.114(2) | 1.937(4) | 0.56 | 36 |
| [Fe(TpivPP)(O₂CCH₃)]⁻ | 2.107(2) | 2.034(3) | 0.55 | 36 |

$^a$ Average Fe−N$_p$ distance. $^b$ Value in Å. $^c$ Large error owing to a disordered ligand. $^d$ This work.

calculations were performed with BP86/TZVP, BP86/TZVP with the larger CP(PPP) basis set[29] on iron, and B3LYP/TZVP again using CP(PPP) for iron. Here, B3LYP is Becke's three-parameter hybrid functional.[30] The Mössbauer isomer shifts were obtained from the calculated total electron densities at the iron nucleus using empirical correlations established by Neese and co-workers.[31] Orbitals were plotted using GaussView (University of Michigan).

## Results and Analysis

**X-ray Structure.** The structure of the [Fe(TPP)Cl]⁻ anion is illustrated in the ORTEP diagram of Figure 3. The anion has many common features with other anionic high-spin five-coordinate iron(II) porphyrinates including the large values of Fe−N$_p$ and the large iron out-of-plane displacements. Selected values are compared in Table 1.[32−36] The strong similarity of [Fe(TPP)Cl]⁻ and [Fe(TpivPP)Cl]⁻ is to be noted. Also to be noted are the common features with the imidazolate structures

(29) (a) Neese, F. *Inorg. Chim. Acta* **2002**, *337*, 181. (b) Sinnecker, S.; Slep, L. D.; Bill, E.; Neese, F. *Inorg. Chem.* **2005**, *44*, 2245.
(30) (a) Becke, A. D. *J. Chem. Phys.* **1993**, *98*, 5648. (b) Lee, C.; Yang, W.; Parr, R. G. *Phys. Rev. B* **1988**, *37*, 785.
(31) Römelt, M.; Ye, S.; Neese, F. *Inorg. Chem.* **2009**, *48*, 784.
(32) Schappacher, M.; Weiss, R. R.; Montiel-Montoya, R.; Gonser, U.; Bill, E.; Trautwein, A. *Inorg. Chim. Acta* **1983**, *78*, L9.
(33) Mandon, D.; Ott-Woelfel, F.; Fischer, J.; Weiss, R.; Bill, E.; Trautwein, A. X. *Inorg. Chem.* **1979**, *101*, 2442.
(34) Nasri, H.; Ellison, M. K.; Shaevitz, B.; Gupta, G. P.; Scheidt, W. R. *Inorg. Chem.* **2006**, *45*, 5284.
(35) Caron, C.; Mitschler, A.; Riviere, G.; Ricard, L.; Schappacher, M.; Weiss, R. *J. Am. Chem. Soc.* **1979**, *101*, 7401.
(36) Nasri, H.; Fischer, J.; Weiss, R.; Bill, E.; Trautwein, A. *J. Am. Chem. Soc.* **1987**, *109*, 2549.

**Figure 4.** Parallel-mode X-band EPR spectra of (A) Fe(TPP)(2-MeHIm)], powder; (B) [Fe(TPP)(2-MeHIm)]₂·2-MeHIm, powder; K(222)[Fe(TPP)(2-MeIm⁻)], 6 mM in (C) chlorobenzene and (D) powder; K(222)[Fe(OEP)(2-MeIm⁻)], 6 mM in (E) chlorobenzene and (F) powder. Experimental conditions: temperature 2 K; microwave power, 0.02 mW at 9.3(1) GHz. Simulation parameters (F, dashed line): $S = 2$, $D = -8$ cm⁻¹, $E/D = 0.10$, $\sigma(E/D) = 0.02$, $g_z = 2.26$.

that were schematically depicted in Figure 2. These include the larger Fe−N$_p$ and Fe out-of-plane displacements, all distinctly different from those of the imidazole complexes. Complete experimental details and experimental results are given in the Supporting Information.

**EPR Spectra.** Figure 4 shows parallel-mode X-band EPR spectra of imidazole- and imidazolate-ligated iron(II) porphyrinates. All species display signals near $g = 9$ indicative of an $S = 2$ state. Solution samples of [Fe(TPP)(2-MeHIm)] and [Fe(TPP)(2-MeHIm)]₂·2-MeHIm did not show parallel-mode EPR signals. The absence of a solution spectrum is probably the result of modest intermolecular interactions in solution. The spectrum of [Fe(TPP)(2-MeHIm)] (Figure 4A) is nearly identical to that of the sample of [Fe(TPP)(2-MeHIm)]₂·2-MeHIm (Figure 4B) containing the two independent molecules: [Fe(TPP)(2-MeHIm)] and hydrogen-bonded [Fe(TPP)(2-MeHIm)]. This result indicates that the hydrogen-bonded [Fe(TPP)(2-MeHIm)] molecule does not produce an EPR signal, presumably due to large $D$ and $E/D$ values of this molecule. For large $D$ and $E/D$, the energy spacing between all spin levels may be too large to observe transitions at the X-band frequency. The temperature dependence of the EPR signal of both samples is shown in Figure 5B, plotted as signal amplitude (base-to-trough) times temperature. For $T > 20$ K, signal broadening makes determination of the amplitude unreliable. Both samples show the same trend in signal amplitude with temperature: the signals originate from an excited state doublet. The theoretical curve is the percent population of the uppermost doublet of an $S = 2$ system with $D = +0.9$ cm⁻¹ and $E/D = 0.1$. However, it is not possible to quantitatively simulate this signal with these zero-field parameters. The simulation of the signal from the ground doublet with these parameters matches the spectrum and agrees with the sample amount, but this doublet does not reproduce the temperature dependence shown in Figure 5B. Thus, we conclude that the magnetic properties of this spin system are not adequately described by a spin Hamiltonian formalism. A similar problem is known for the description of the EPR data

**Figure 5.** Temperature dependence of the EPR signals of (A) K(222)[Fe(OEP)(2-MeIm$^-$)], (B) [Fe(TPP)(2-MeHIm)] (×), and (B) [Fe(TPP)(2-MeHIm)]$_2$·2-MeHIm (+) plotted as signal amplitude times temperature. The theoretical curves are the percent populations of an $S = 2$ ($E/D = 0.1$) system for (A) the lowermost doublet with $D = -8$ cm$^{-1}$, and (B) the uppermost doublet with $D = +0.9$ cm$^{-1}$. The $D$-value of [Fe(TPP)(2-MeHIm] is estimated from the temperature dependence of the EPR signal.

of deoxymyoglobin. Deoxymyoglobin shows an EPR spectrum similar to that of these [Fe(TPP)(2-MeHIm)] complexes, and its characteristics are also not adequately described with a spin Hamiltonian.[37]

The EPR spectra from the imidazolate-ligated complex K(222)[Fe(TPP)(2-MeIm$^-$)] are more complicated (Figure 4C, D). It appears that both solution and powder samples have multiple species present with features near $g = 14$ and 9. The temperature dependence of these signals is complicated by the presence of multiple species, but overall suggests $D < 0$ with signals originating from the ground doublet. In contrast, the EPR spectrum of imidazolate-ligated K(222)[Fe(OEP)(2-MeIm$^-$)] shows a single species in the solid state (Figure 4F). A plot of the signal times temperature is shown in Figure 5A. The theoretical curve is percent population for the lowermost doublet of an $S = 2$ system with $D = -8$ cm$^{-1}$ and $E/D = 0.1$. A simulation using these parameters for the ground doublet is overlaid on the spectrum (dashed line). This simulation is in quantitative agreement with the spectrum and the sample amount. The solution sample of this complex (Figure 4E) also shows multiple species.

We can draw two conclusions from the results described here. First, the imidazole- and imidazolate-ligated iron(II) porphyrin complexes exhibit very different electronic properties. Based on the determination of the sign and magnitude of the $D$-value, we can conclude that the electronic structures of these complexes must be different. Second, these complexes show a parallel-mode EPR signal indicative of electronic properties with significant distortion from axial symmetry. This finding correlates well with crystallographic data which shows that the Fe$-$N$_{Im}$ bond is not along the heme normal.

**Mössbauer Spectra.** Mössbauer spectra for both imidazole and imidazolate-ligated derivatives have been measured in strong applied magnetic fields and previously reported.[11–15] The two classes were found, without question, to have opposite values for the sign of the quadrupole splitting. Quadrupole splitting values for the imidazole-ligated derivatives were in the range of 1.96 to 2.40 mm/s at 4.2 K with negative sign for the value, whereas those for imidazolate were in the range of 3.60 to 3.71 mms/s and with positive signs. However in the initial fits, the sign of the $D$-value was not found to be distinctly different in the two classes. The apparent difficulty of assigning the sign of $D$ was commented on in our earliest work on imidazole derivatives.[11] Even so, in view of the integer-spin EPR results,
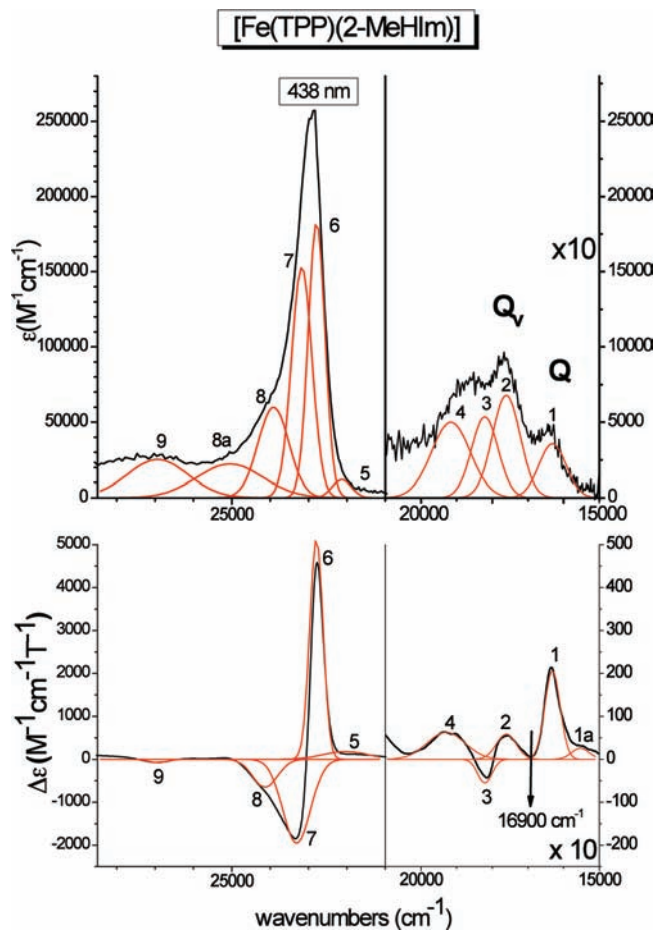


**Figure 6.** Electronic spectra of [Fe(TPP)(2-MeHIm)] (class N). (Top) UV$-$vis spectrum measured in CH$_2$Cl$_2$ at room temperature. (Bottom) MCD **C**-Term spectrum measured in toluene/CH$_2$Cl$_2$ (1:1) at 2 K. The red lines represent a correlated fit of these data (cf. Table 3A).

the fitting of the previously obtained Mössbauer spectra have been reexamined to determine if the Mössbauer spectra will show sensitivity to the sign of $D$ for the two classes. Our conclusion remains that the sign of $D$ is ambiguous in the fits. Notwithstanding the ambiguity in the sign determination, good simulations of the Mössbauer data can be obtained with the use of the $E/D$ and $D$ parameters given above from the EPR measurements. When there are large values of $D$, in systems that will be EPR silent, the high-field Mössbauer data can unambiguously determine the sign of $D$. However, for the smaller $D$ values seen in the imidazolate compounds, integer-spin EPR is crucial for the determination of this sign.

**Magnetic Circular Dichroism Spectra.** Figure 6 shows the absorption and low-temperature MCD spectra of [Fe(TPP)(2-MeHIm)] (Class **N**, neutral axial ligand) together with Gaussians obtained from a correlated fit of these data. The obtained band positions are listed in Table 3A. These spectra show four relatively intense features in the region of the Q and Q$_v$ bands, plus the Soret band around 23000 cm$^{-1}$, which is resolved into three features in MCD. As shown by one of us previously, the Soret, Q, and Q$_v$ bands of simple metalloporphyrins should give rise to a derivative-shaped **C**-term signal at low-temperature in MCD due to a low-symmetry splitting of the porphyrin $E_g$ ($\pi^*$) LUMO of the complexes.[38] This causes the Soret, Q, and Q$_v$ excited states, which have E$_u$ symmetry in D$_{4h}$, to split into two

(37) Hendrich, M. P.; Debrunner, P. G. *Biophys. J.* **1989**, *56*, 489.

components, and correspondingly, two bands are observed for the Soret, Q, and $Q_v$ transitions in MCD. Importantly, due to excited state spin−orbit coupling, the two components of these features show opposite signs, and hence, the Soret, Q, and $Q_v$ transitions each give rise to a derivative shaped "pseudo-**A**" **C**-term signal in MCD at low (lq. helium) temperature. Additionally, since $Q_v$ is the vibronic band of Q, it should appear about 1250 cm$^{-1}$ to higher energy of Q as determined by Gouterman.[39] With this in mind, the electronic spectra of [Fe(TPP)(2-MeHIm)] can be readily understood. At low energy, one component of the Q-band is observed at 16315 cm$^{-1}$ (band 1). The $Q_v$ band corresponds to the pseudo-**A** signal at 17608 and 18210 cm$^{-1}$ (bands 2 and 3). This indicates a relatively large splitting of the two components of the Q excited state of about 600 cm$^{-1}$ as determined from $Q_v$. The MCD bands 1 and 2 correspond to the first component of the Q and $Q_v$ excited states, respectively, as evident from (a) their energetic separation of 1293 cm$^{-1}$, which is very close to the predicted value of ~1250 cm$^{-1}$, and (b) the fact that both have positive MCD intensity, which means that 2 must be the vibronic band of 1. This raises one question: where is the negative, second component of the Q-band located that corresponds to band 3 of $Q_v$? Using the observed energy difference between bands 2 and 3 of about 600 cm$^{-1}$, the energy of the negative Q component is estimated to ~16900 cm$^{-1}$, as indicated in the MCD spectrum in Figure 6. One circumstance that could contribute to the absence of this feature in the MCD spectrum is the large ~600 cm$^{-1}$ splitting of the Q state, which places this feature just in between the positive bands 1 and 2. Since this feature must be negative, its MCD intensity might then cancel out against these positive features (cf. analysis of the MCD data of [Fe(TPP)(2-MeIm$^-$)]$^-$ below). In the case of the Soret band, the negative component is split into two bands as shown in Figure 6, which is not unusual, since other porphyrin $\pi \rightarrow \pi^*$ transitions appear in this region. These can specifically mix with just one component of the Soret band, and in this way, give rise to the experimentally observed three-band pattern for the Soret transition. This has recently been discussed in detail for [Fe$^{III}$(TPP)Cl] by one of us.[40] The main components of the Soret feature (bands 6 and 7) are located at 22795 and 23310 cm$^{-1}$, respectively, which is consistent with the observed large energy splitting between the two components of the $Q_v$ band mentioned above. Importantly, the molar MCD intensity of [Fe(TPP)(2-MeHIm)] is surprisingly large, and corresponds to "normal" low-spin ferric hemes as discussed in ref 40.

Figure 7 shows the electronic spectra of [Fe(TPP)(2-MeIm$^-$)]$^-$ (Class **A**, anionic axial ligand) for comparison. In this case, the Soret, Q, and $Q_v$ features are readily identified from the MCD spectrum via their pseudo-**A** **C**-term behavior. Table 3B summarizes the obtained band positions from a correlated fit of these data. Here, bands 2 and 3, observed at 16206 and 16432 cm$^{-1}$ in MCD, belong to the Q transition, and bands 4 and 5, located at 17308 and 17640 cm$^{-1}$ in MCD, are identified with $Q_v$. The energy differences between the corresponding features 2 and 4 (negative) and 3 and 5 (positive)
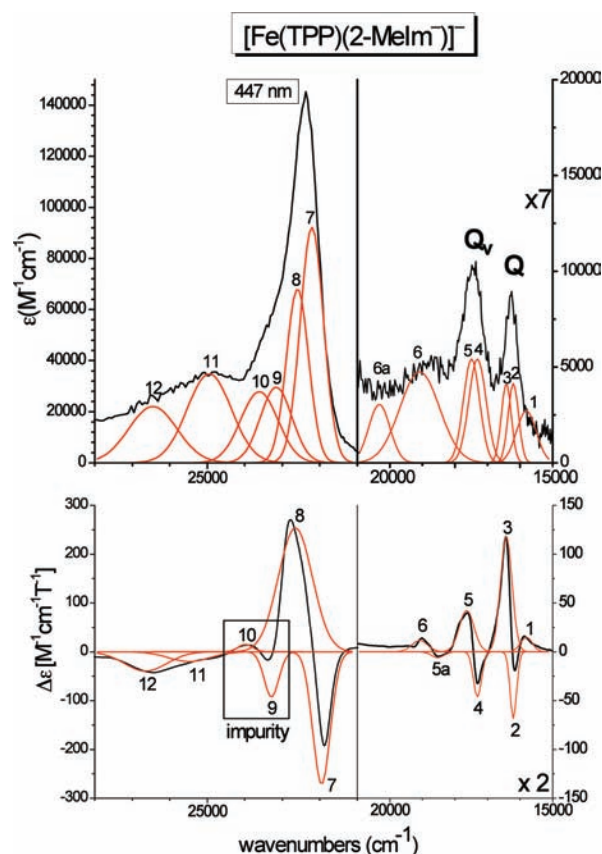


**Figure 7.** Electronic spectra of [Fe(TPP)(2-MeIm$^-$)]$^-$ (class **A**). (Top) UV−vis spectrum measured in CH$_2$Cl$_2$ at room temperature. (Bottom) MCD **C**-Term spectrum measured in toluene/CH$_2$Cl$_2$ (1:1) at 2 K. The red lines represent a correlated fit of these data (cf. Table 3B).

**Table 2.** Comparison of Observed and Calculated Structural Parameters for High-Spin Iron(II) Porphyrinates

| complex | $\langle Fe-N_p \rangle^{a,b}$ | Fe$-$Ax$^b$ | $\Delta N_4{}^b$ | $\phi^c$ | ref |
|---|---|---|---|---|---|
| [Fe(TPP)(2-MeHIm)]-Obsd | 2.073 (9) | 2.127 | 0.32 | 24 | 10 |
| -Calcd | 2.090 (8) | 2.183 | 0.35 | 18.3 | tw$^d$ |
| [Fe(TPP)(2-MeIm$^-$)]$^-$-Obsd | 2.118 (13) | 2.056 | 0.56 | 23.4 | 12 |
| -Calcd | 2.119 (17) | 2.048 | 0.50 | 1 | tw$^d$ |
| -Calcd-fixed | 2.118 (16) | 2.051 | 0.51 | 23 | tw$^d$ |
| [Fe(TPP)Cl]$^-$-Obsd | 2.113 (19) | 2.340 | 0.56 | − | tw$^d$ |
| -Calcd | 2.119 (19) | 2.300 | 0.51 | − | tw$^d$ |

$^a$ Average value. $^b$ Value in Å. $^c$ Dihedral angle between imidazole plane and closest Fe$-N_p$ vector, value in degrees. $^d$ This work.

are 1102 and 1208 cm$^{-1}$, which is in good agreement with the predicted value of ~1250 cm$^{-1}$ mentioned above. The relatively low value of 1102 cm$^{-1}$ is due to the fact that the position of band 2 is not well-defined in the fit. Interestingly, the energy splitting between the two components of Q and $Q_v$ is only about 200−300 cm$^{-1}$, which is distinctively smaller than in the case of [Fe(TPP)(2-MeHIm)]. The intensity of the negative band 2 is surprisingly low, but this can be attributed to the fact that this feature is close to the positive bands 1 and 3, and hence, the intensity of band 2 is canceled out to a large extent, as illustrated by the fit of this feature in Figure 7. This is similar to the case of the missing negative component of the Q-band in [Fe(TPP)(2-MeHIm)] discussed above. Due to the lability of [Fe(TPP)(2-MeIm$^-$)]$^-$ with the imidazolate ligand, it was not possible to prepare MCD samples of this compound without the presence of a slight amount of presumably a ferric impurity. Comparison of different samples shows that bands 9 and 10

(38) (a) Praneeth, V. K. K.; Näther, C.; Peters, G.; Lehnert, N. *Inorg. Chem.* **2006**, *45*, 2795. (b) Lehnert, N., Electron Paramagnetic Resonance and Low-Temperature Magnetic Circular Dichroism Spectroscopy of Ferrous Heme Nitrosyl. In *The Smallest Biomolecules: Perspectives on Heme-Diatomic Interactions*; Ghosh, A., Ed.; Elsevier: Amsterdam, 2008; Chapter 6, pp 147−171.

(39) Gouterman, M. in The Porphyrins; Dolphin, D., Ed Academic: New York, 1979, Vol. III Part A, pp1−156.

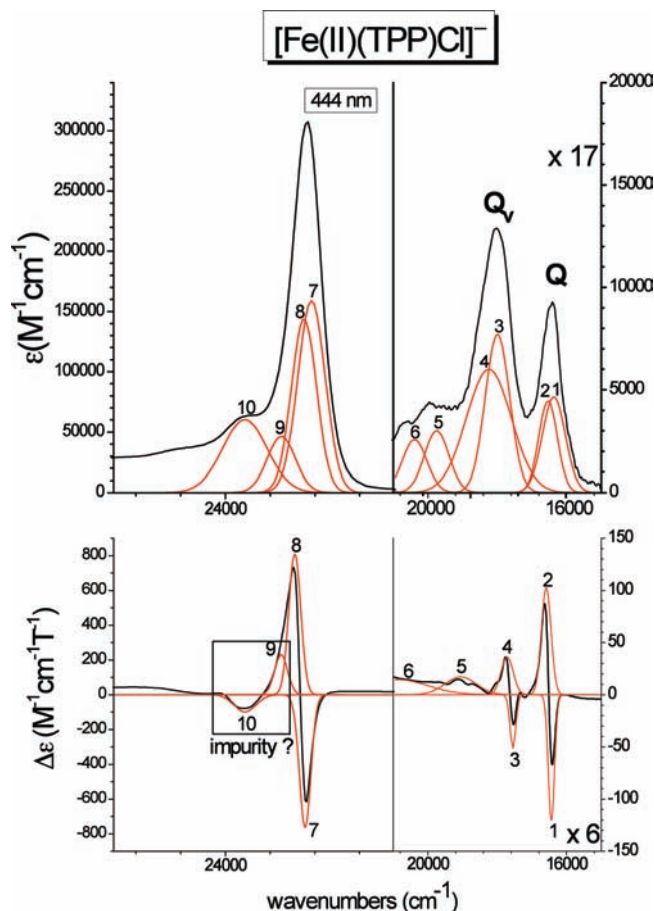(40) Paulat, F.; Lehnert, N. *Inorg. Chem.* **2008**, *47*, 4963.

***Table 3.*** Correlated Fit of the UV−Vis Absorption and MCD Spectra Shown in Figures 6−8[a]

| no. | MCD position | $\Delta\epsilon$(M$^{-1}$cm$^{-1}$T$^{-1}$) | UV−vis position | $\epsilon$(M$^{-1}$cm$^{-1}$) |
|---|---|---|---|---|
| | | A. [Fe(TPP)(2-MeHIm)] | | |
| 1a | 15531 | 26.0 | − | − |
| 1 | 16315 | 206.8 | 16315 | 3571.4 |
| 2 | 17608 | 58.5 | 17608 | 6785.7 |
| 3 | 18210 | −55.5 | 18210 | 5357.1 |
| 4 | 19295 | 62.9 | 19160 | 5000.1 |
| 5 | 22031 | 180.4 | 22131 | 12142.9 |
| 6 | 22795 | 5131.5 | 22790 | 183000.0 |
| 7 | 23310 | −1956.4 | 23176 | 153000.0 |
| 8 | 24134 | −649.4 | 23912 | 6000.0 |
| 8a | − | − | 25048 | 22302.3 |
| 9 | 26932 | −77.1 | 26934 | 25289.1 |
| | | B. [Fe(TPP)(2-MeIm$^-$)]$^-$ | | |
| 1 | 15807 | 15.0 | 15807 | 2716.0 |
| 2 | 16206 | −68.6 | 16206 | 4142.9 |
| 3 | 16432 | 118.51 | 16432 | 4142.9 |
| 4 | 17308 | −46.3 | 17308 | 5428.6 |
| 5 | 17640 | 42.3 | 17491 | 5428.6 |
| 5a | 18528 | −6.0 | − | − |
| 6 | 19082 | 11.6 | 19082 | 4745.9 |
| 6a | − | − | 20321 | 3048.8 |
| 7 | 21950 | −271.7 | 22209 | 92104.2 |
| 8 | 22650 | 253.7 | 22592 | 68100.6 |
| 9 | 23288 | −92.9 | 23162 | 29607.5 |
| 10 | 23983 | 14.9 | 23612 | 27830.6 |
| 11 | 25482 | −20.1 | 24946 | 34796.6 |
| 12 | 26642 | −39.4 | 26450 | 22051.0 |
| | | C. [Fe(TPP)Cl]$^-$ | | |
| 1 | 16438 | −120.2 | 16251 | 4642.9 |
| 2 | 16587 | 102.3 | 16372 | 4464.3 |
| 3 | 17547 | −51.4 | 17434 | 7712.8 |
| 4 | 17714 | 36.2 | 17614 | 6000.1 |
| 5 | 19057 | 17.1 | 19710 | 2571.4 |
| 6 | 20864 | 14.4 | 20527 | 2071.4 |
| 7 | 22576 | −762.4 | 22460 | 159000.0 |
| 8 | 22760 | 807.7 | 22595 | 144000.0 |
| 9 | 23005 | 233.9 | 23005 | 46428.5 |
| 10 | 23652 | −98.7 | 23652 | 60135.4 |

[a] For the fit, the *minimum number* of Gaussians has been used. If a band can be identified from the MCD spectrum, but no corresponding band is necessary to fit the absorption spectrum, then the absorption data is not fit with this feature. Hence, in very few cases, bands appear in the correlated fit of the MCD spectra, but not in the fit of the absorption spectra (or vice versa).

actually belong to this impurity. Therefore, the Soret band of [Fe(TPP)(2-MeIm$^-$)]$^-$ is assigned to bands 7 and 8, observed at 21950 and 22650 cm$^{-1}$, respectively. Due to the strong overlap of bands 7−9, the absolute energies of these features are not well-defined. *The most striking difference in the MCD spectra of complexes [Fe(TPP)(2-MeHIm)] and [Fe(TPP)(2-MeIm$^-$)]$^-$ is the significantly lower molar MCD intensity in the case of [Fe(TPP)(2-MeIm$^-$)]$^-$ by one order of magnitude.* This difference relates to the electronic structures of the complexes, and is further analyzed below (cf. DFT Sections). In addition, the signs of the Soret, Q, and Q$_v$ MCD bands are opposite in [Fe(TPP)(2-MeIm$^-$)]$^-$ compared to [Fe(TPP)(2-MeHIm)], i.e. [Fe(TPP)(2-MeHIm)] shows the sequence $+\Delta\epsilon/(-\Delta\epsilon)/+\Delta\epsilon/-\Delta\epsilon/+\Delta\epsilon/-\Delta\epsilon$ (from lower to higher energy: Q − Q$_v$− Soret), whereas [Fe(TPP)(2-MeIm$^-$)]$^-$ (and [Fe(TPP)Cl]$^-$, vide infra) exhibits the sequence $-\Delta\epsilon/(+\Delta\epsilon)/-\Delta\epsilon/+\Delta\epsilon/-\Delta\epsilon/+\Delta\epsilon$. As

(41) (a) Michl, J. *J. Am. Chem. Soc.* **1978**, *100*, 6801 (and the other 16 articles in this issue). (b) Mack, J.; Stillman, M. J.; Kobayashi, N. *Coord. Chem. Rev.* **2007**, *251*, 429.

**Figure 8.** Electronic spectra of [Fe(TPP)Cl]$^-$ (class **A**). Top: UV−vis spectrum measured in CH$_2$Cl$_2$ at room temperature. Bottom: MCD C-Term spectrum measured in toluene/ CH$_2$Cl$_2$ (1:1) at 2 K. The red lines represent a correlated fit of these data (cf. Table 3C).

shown by Michl, this can be explained by a change in the relative HOMO (porphyrin $A_{1u}$, $A_{2u}$) and LUMO (porphyrin $E_g$) splitting of the porphyrin ring,[41] where the sequence observed for [Fe(TPP)(2-MeHIm)] is associated with $\Delta$(LUMO) ≫ $\Delta$(HOMO). [Fe(TPP)(2-MeIm$^-$)]$^-$ (and [Fe(TPP)Cl]$^-$) then correspond to the $\Delta$(HOMO) ≫ $\Delta$(LUMO) case.

Finally, Figure 8 shows the absorption and MCD data of complex [Fe(TPP)Cl]$^-$ (class **A**). As in the case of [Fe(TPP)(2-MeIm$^-$)]$^-$, clean pseudo-**A** C-term signals are observed for Q, Q$_v$, and the Soret band, which can therefore readily be identified from the spectra. The Q-band corresponds to bands 1 and 2 observed at 16438 and 16587 cm$^{-1}$, respectively. The vibronic Q$_v$ transition is identified with bands 3 and 4 at 17547 and 17714 cm$^{-1}$. Therefore, [Fe(TPP)Cl]$^-$ shows the smallest splitting between the two components of the Q excited state of only ~150 cm$^{-1}$. The energy difference between components 1 and 2 of Q and Q$_v$ is 1109 (bands 1 and 3) and 1127 cm$^{-1}$ (bands 2 and 4), respectively, which is in good agreement with the predicted value of ~1250 cm$^{-1}$ (vide supra). The main components of the Soret band are assigned to bands 7 and 8 at 22576 and 22760 cm$^{-1}$, respectively, again reflecting the very small energy splitting between the two components of the E$_u$ excited states as observed for Q. Band 9 could either correspond to a third Soret component as observed for [Fe(TPP)(2-MeHIm)], or an impurity as in the case of [Fe(TPP)(2-MeIm$^-$)]$^-$. The latter explanation is the most likely, based on the observed pseudo-**A** behavior of bands 9 and 10 in [Fe(TPP)Cl]$^-$, which is very

similar to the MCD features of the impurity observed for [Fe(TPP)(2-MeIm⁻)]⁻. *Importantly, the molar MCD intensity of [Fe(TPP)Cl]⁻ is again much lower compared to [Fe(TPP)(2-MeHIm)]*. This indicates that this difference in the total molar MCD intensity[42] between Class **N** and Class **A** high-spin ferrous hemes constitutes a general trend, and can be employed to distinguish between the two classes of compounds. Correspondingly, these two classes must differ significantly in their electronic structures, which would then explain the apparent difference in total MCD intensity. The experimentally determined order in MCD intensity is: [Fe(TPP)(2-MeHIm)] ≫ [Fe(TPP)Cl]⁻ > [Fe(TPP)(2-MeIm⁻)]⁻ as evident from Figures 6−8. The electronic structures of these complexes are compared in detail below.

**Density Functional Theory (DFT) Calculations: Geometry Optimizations.** To determine the electronic structural differences between the two different classes of five-coordinate, high-spin ferrous hemes, we have fully optimized the geometries of the complexes [Fe(TPP)(2-MeHIm)], [Fe(TPP)(2-MeIm⁻)]⁻, and [Fe(TPP)Cl]⁻ using BP86/TZVP without any simplifications. Figures S1−S3 (Supporting Information) show core diagrams of the fully optimized structures including important bond lengths. In the case of [Fe(TPP)(2-MeHIm)], the Fe−$N_p$ and Fe−$N_{Im}$ distances of 2.090 (averaged) and 2.183 Å, respectively, are somewhat on the large side of the range of values observed for imidazole complexes (Table 2), but are still in reasonably good agreement with experiment. The out-of-plane displacement, $\Delta N_4$, of iron of 0.35 Å and the orientation of the imidazole relative to the porphyrin plane (dihedral angle $\phi = 18°$) are in excellent agreement with the crystal structure of [Fe(TPP)(2-MeHIm)] (exp. values: 0.32 Å and 24°, respectively). The out-of-plane distortions of the TPP ring in both the experimental and calculated structures are complex, and correspond to a combination of different types of distortions[43] leading to $C_1$ symmetries of the cores. As evident from Figure S1 (Supporting Information), ruffling is more dominant in the calculated structure compared to the experimental result. In comparison, the calculated Fe−$N_p$ and Fe−$N_{Im}$ distances of 2.119 (averaged) and 2.048 Å, respectively, for the imidazolate complex [Fe(TPP)(2-MeIm⁻)]⁻ are in excellent agreement with experiment (Table 2). This is also true for the calculated out-of-plane displacement $\Delta N_4$ of iron, which is 0.50 Å (exp. value: 0.56 Å). The largest deviation in the case of [Fe(TPP)(2-MeIm⁻)]⁻ is observed for the orientation of the imidazolate: the calculated value for $\phi = 1°$ is smaller compared to $\phi = 23°$ from experiment. We therefore recalculated the structure of [Fe(TPP)(2-MeIm⁻)]⁻ where the angle $\phi$ was fixed at 23° ([Fe(TPP)(2-MeIm⁻)]⁻ (fixed)). The structure obtained from this treatment is only +0.7 kcal/mol higher in energy than [Fe(TPP)(2-MeIm⁻)]⁻, and is shown in the Supporting Information, Figure S2. Besides the change in the dihedral angle, the other geometric

(42) It would be advantageous to actually compare molar MCD **C**-term intensities here instead of the total molar MCD intensities, since the latter also include contributions form the MCD **A**- and **B**-terms. However, as shown in ref 40, MCD measurements at room temperature are required to determine the absolute A- and B-term intensities. The frozen glasses applied here do not allow these data to be measured, since the glasses disintegrate above 150 K. Data taken at ~100 K still show very significant **C**-term contributions.

(43) (a) Shelnutt, J. A.; Song, X.-Z.; Ma, J.-G.; Jia, S.-L.; Jentzen, W.; Medforth, C. *J. Chem. Soc. Rev.* **1998**, 31. (b) Scheidt, W. R. Systematics of the Stereochemistry of Porphyrins and Metalloporphyrins. In *The Porphyrin Handbook*; Kadish, K. M.; Smith, K. M.; Guilard, R., Eds.; Academic Press: San Diego, 2000; Vol. 3, Chapter 16, pp 49−112.

**Table 4.** Summary of the Experimental EPR and Mössbauer Results for the Investigated High-Spin Ferrous Heme Complexes

| | [Fe(TPP)(2-MeHIm)] | [Fe(TPP)(2-MeIm⁻)]⁻ | [Fe(TpivPP)Cl]⁻ |
|---|---|---|---|
| $D$ (cm⁻¹) | +0.9[a] | −8[b] | n/a[c] |
| $\delta$ (mm/s) | 0.85 | 1.00 | 1.01 |
| $\Delta E_q$ (mm/s) | −1.95 | +3.60 | 4.36 |
| $\eta$ | 0.8 | 0.02 | n/a[c] |

[a] $D = -5.0$ cm⁻¹ had initially been obtained by Lang et al. (*J. Chem. Phys.* **1979**, *71*, 4899) from Mössbauer spectroscopy at 6T. This value was later corrected to a positive $D$ of about 5−30 cm⁻¹ based on variable-field Mössbauer measurements by Scheidt and co-workers (*J. Am. Chem. Soc.* **2005**, *127*, 5675). However, Mössbauer fits are not very sensitive to the value of $D$, and hence, the EPR-based value presented here is much more reliable. [b] Determined for [Fe(OEP)(2-MeIm⁻)]⁻. [c] Not available

parameters of [Fe(TPP)(2-MeIm⁻)]⁻ (fixed) are very similar compared to the fully optimized structure of [Fe(TPP)(2-MeIm⁻)]⁻. More importantly, the electronic structures of [Fe(TPP)(2-MeIm⁻)]⁻ and [Fe(TPP)(2-MeIm⁻)]⁻ (fixed) are similar as discussed below. The nonplanar distortions of the TPP core in the experimental and calculated structures of [Fe(TPP)(2-MeIm⁻)]⁻ are again complex. The experimental core conformation of [Fe(TPP)(2-MeIm⁻)]⁻ shows a clear saddling contribution. In the case of the calculated structures, the imidazolate complexes [Fe(TPP)(2-MeIm⁻)]⁻ and [Fe(TPP)-(2-MeIm⁻)]⁻ (fixed) show pronounced contributions of the doming distortion, but less saddling. Finally, the calculated Fe−$N_p$ and Fe−Cl distances of 2.119 (averaged) and 2.300 Å, respectively, for the chloride complex [Fe(TPP)Cl]⁻ are again in excellent agreement with experiment (Table 2). The calculated out-of-plane displacement $\Delta N_4$ is 0.51 Å, which also compares well with experiment (exp. value for [Fe(TPP)Cl]⁻: 0.56 Å). As observed before, both the experimental and calculated structures of [Fe(TPP)Cl]⁻ show complex nonplanar distortions of the porphyrin core that differ somewhat between theory and experiment. The distortion observed in the crystal structure corresponds mostly to ruffling and doming, whereas the calculated structure does not predict the ruffling contribution.

In summary, the DFT calculations are able to reproduce the geometries of the high-spin Fe(II) coordination groups well in the three complexes, including Fe−ligand bond lengths, relative orientations of imidazole and imidazolate, and, importantly, the out-of-plane displacement of iron. The cores of the TPP ligands show strong low-symmetry ($C_1$) distortions, and differences are observed in the core conformations between theory and experiment. However, as a comparison of [Fe(TPP)(2-MeIm⁻)]⁻ and [Fe(TPP)(2-MeIm⁻)]⁻ (fixed) shows, the effects of these differences on the electronic structure of the iron(II) center are very small.

**Calculation of Zero Field Splitting and Mössbauer Parameters from DFT.** As described above, the EPR and Mössbauer measurements have identified dramatic differences in the magnitude and sign of the axial zero field splitting parameter $D$ and the Mössbauer quadrupole splitting $\Delta E_q$ between high-spin ferrous heme complexes of classes **N** and **A**, as summarized in Table 4. In particular, complexes with neutral imidazole ligands (class **N**) like [Fe(TPP)(2-MeHIm)] show negative quadrupole splittings $\Delta E_q$ and large asymmetry parameters $\eta$, whereas complexes with axial anionic imidazolate or chloride ligands (Class **A**) like [Fe(TPP)(2-MeIm⁻)]⁻ and [Fe(TPP)Cl]⁻ exhibit a positive $\Delta E_q$ and a small $\eta$. Since $\Delta E_q$ reflects the electron distribution of iron in the ground state, these differences indicate that compounds of classes **N** and **A** differ

**Table 5.** Summary of the DFT-Calculated EPR and Mössbauer Parameters for High-Spin Ferrous Heme Complexes Using Fully Optimized Structures from BP86/TZVP

| | BP86/TZVP + CP(PPP) on Fe | | B3LYP/TZVP + CP(PPP) on Fe | |
| --- | --- | --- | --- | --- |
| | [Fe(TPP)(2-MeHIm)] | [Fe(TPP)(2-MeIm⁻)]⁻ | [Fe(TPP)(2-MeHIm)] | [Fe(TPP)(2-MeIm⁻)]⁻ |
| g-values | 2.029 | 2.010 | 2.041 | 2.018 |
| | 2.036 | 2.035 | 2.056 | 2.047 |
| | 2.064 | 2.050 | 2.075 | 2.058 |
| g-iso | 2.043 | 2.032 | 2.058 | 2.041 |
| $D$ (cm$^{-1}$) | −3.74 | +2.55 | −4.74 | −6.21 |
| $E/D$ | 0.31 | 0.21 | 0.27 | 0.16 |
| $\rho$ (o) (au$^{-3}$) | 11826.88925 | 11826.97657 | 11815.71193 | 11815.63672 |
| $\delta$ (mm/s) | 0.738 | 0.700 | 0.761 | 0.789 |
| $\Delta E_q$ (mm/s) | −2.213 | +2.213 | 2.783 | +3.772 |
| $\eta$ | 0.761 | 0.391 | 0.992 | 0.066 |

**Table 6.** Summary of the DFT-Calculated EPR and Mössbauer Parameters for High-Spin Ferrous Heme Complexes Based on the Experimentally Observed Structures

| | BP86/TZVP + CP(PPP) on Fe | |
| --- | --- | --- |
| | [Fe(TPP)(2-MeHIm)] | [Fe(TPP)(2-MeIm⁻)]⁻ |
| g-values | 2.0114 | 2.0002 |
| | 2.0409 | 2.0296 |
| | 2.0739 | 2.0802 |
| g-iso | 2.0421 | 2.0367 |
| $D$ (cm$^{-1}$) | +3.4077 | −2.2767 |
| $E/D$ | 0.2917 | 0.3174 |
| $\rho$ (o) (au$^{-3}$)] | 11827.10921 | 11827.10552 |
| $\delta$ (mm/s) | 0.645 | 0.646 |
| $\Delta E_q$ (mm/s) | −2.313 | +2.335 |
| $\eta$ | 0.751 | 0.141 |

in their electronic ground states. DFT calculations on the optimized structures with either BP86/TZVP (see Table S7, Supporting Information)) or BP86/TZVP using the larger CP(PPP) basis set for iron (see Table 5, left) reproduce this difference in the sign of $\Delta E_q$ and the value of $\eta$ very well. The differences between these two methods are negligible.

Interestingly, our EPR results also show that [Fe(TPP)(2-MeHIm)] and [Fe(OEP)(2-MeIm⁻)]⁻ differ in the sign of the axial zero-field splitting parameter $D$ as shown in Table 4. Because the value of $D$ relates to spin−orbit coupling of the ground state with low-lying excited states, this sign difference in $D$, however, is much less diagnostic for a difference in ground states than is $\Delta E_q$. Using BP86 calculations on the DFT-optimized structures, the sign change of $D$ is again reproduced, but in the opposite way compared to experiment: whereas experimentally, the imidazole complex has a positive $D$ and for the imidazolate complex $D$ is negative, the DFT calculations predict exactly the opposite trend. In order to determine whether this relates to small structural differences between the experimental (crystallographic) and DFT-optimized structures, we then recalculated the EPR and Mössbauer parameters for the observed molecular structures. As shown in Table 6, both the trends in $\Delta E_q$ and in $D$ are now exactly reproduced in the calculations. In addition, the agreement for $\eta$ has also distinctively improved. This indicates that the small deviations in the porphyrin structures as described above are significant for the calculation of $D$, i.e. the excited states energies, whereas the electronic ground state is described well in either case, and $\Delta E_q$ is insensitive to this difference.

Finally, we also tried B3LYP/TZVP calculations (using CP(PPP) on Fe) on the DFT-optimized structures. The results, shown in Table 5, right, do not reproduce the experimental results, that is, no sign change for either $\Delta E_q$ or $D$ is observed. This method is therefore unsuitable. In the following, *the*

*electronic structural differences between class* **N** *and* **A** high-spin ferrous hemes are therefore analyzed based on BP86/TZVP calculations on the crystal structures. As shown in the Supporting Information, the same conclusions about the electronic ground states of these compounds are drawn from the MO diagrams obtained for the DFT-optimized structures. This again emphasizes that the small structural differences between the experimental and optimized structures of the different compounds do not affect the ground states of these complexes in a significant way, as reflected by the similar $\Delta E_q$ values.

**Electronic Structure from DFT.** In all three complexes, iron(II) is in the high-spin state ($S = 2$), and hence, the principal d-electron configuration of the metal is $[t_2]^4[e]^2$ or $[d_{xz}, d_{yz}, d_{xy}]^4$ $[d_{x^2-y^2}, d_{z^2}]^2$. In a spin unrestricted formalism, this means that all $\alpha$-d orbitals are occupied, and in addition, one of the $\beta$-d orbitals is occupied (here, $\alpha$ denotes the majority spin and $\beta$ the minority spin). Correspondingly, the central questions for the electronic structures of the complexes are (a) which one of the three $t_2$-type orbitals carries the $\beta$-electron, and (b) what is the energy sequence of the remaining two unoccupied $\beta$-$t_2$ orbitals. Because of this, the $\beta$-MO diagrams of the three complexes are individually discussed in the following.

Figure 9 shows the frontier $\beta$-MO diagram of [Fe(TPP)(2-MeHIm)], obtained for the observed molecular structure using BP86/TZVP. In this case, the single $\beta$-d electron occupies the bonding combination of the $d_{xz}$ orbital with one component of the unoccupied $E_{(g)}$ LUMO of the porphyrin ring (cf. Figure S4 for porphyrin orbitals, Supporting Information). As can be seen from the contour plot in Figure 9, the ~0.3 Å out-of-plane displacement of iron actually allows for a weak $\sigma$ backbonding interaction between these orbitals. The resulting MO, labeled $d_{xz}\_E_{(g)}$, has 65% $d_{xz}$ character. *Importantly, the $d_{xz}$ orbital is located in the plane of the imidazole ligand.* The $\beta$-$d_{yz}$ orbital is unoccupied, and is found 2221 cm$^{-1}$ higher in energy. Again, this orbital shows a $\sigma$ backbonding interaction with the other component of the $E_{(g)}$ porphyrin LUMO, and the resulting bonding combination is labeled $d_{yz}\_E_{(g)}$ in Figure 9. The $d_{yz}$ orbital is oriented perpendicular to the imidazole plane, and shows an additional $\pi$ bonding interaction with an occupied $\pi$ orbital of the imidazole ligand. The relatively large rhombic splitting between the $d_{xz}$ and $d_{yz}$ orbitals is therefore mostly due to the axial imidazole ligand, and not the splitting of the porphyrin $E_{(g)}$ LUMO caused by the nonplanar distortion of the porphyrin ring (vide supra). Finally, the $d_{xy}$ orbital is nonbonding, and found at highest energy as shown in Figure 9. This orbital sequence with the $d_{xz}$ and $d_{yz}$ orbitals at lower energy than $d_{xy}$ is uncommon for iron porphyrin complexes, but is consistent with the conclusions drawn earlier from Mössbauer spectroscopy.[11] The well-studied low-spin ferric hemes usually
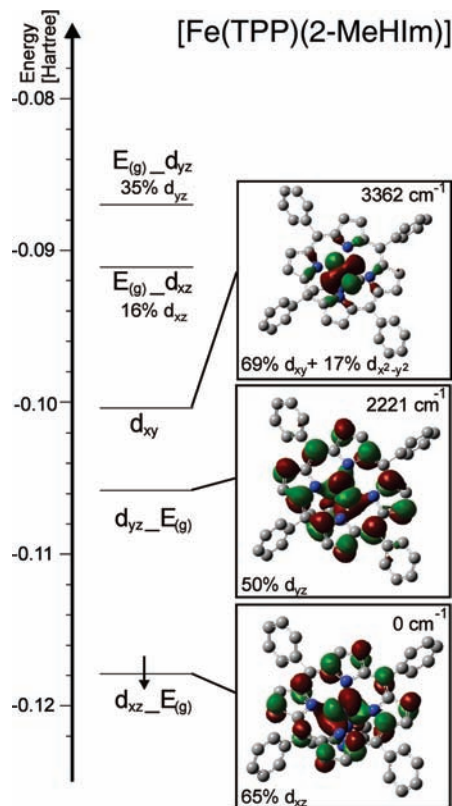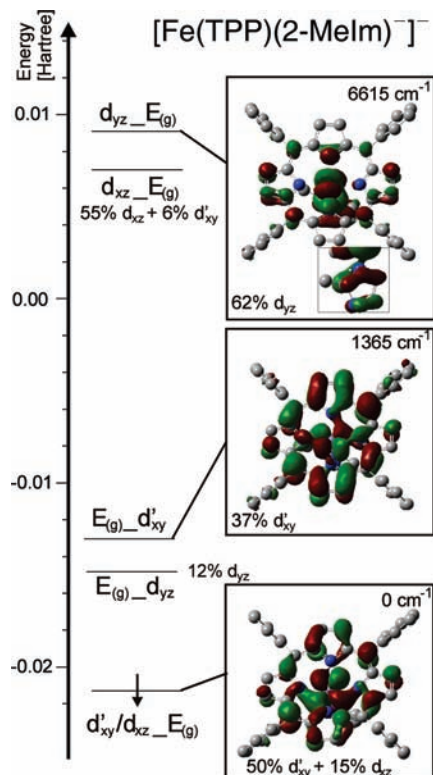
**Figure 9.** Frontier $\beta$-MO diagram of [Fe(TPP)(2-MeHIm)] calculated with BP86/TZVP. The applied coordinate system is chosen such that $x$ and $y$ are located in the porphyrin plane, and $z$ is orthogonal to the porphyrin ring in the direction of the axial ligand. $E_{(g)}$ refers to the LUMO of the porphyrin as shown in Figure S4 (the index g is put in brackets because of the low symmetry of the porphyrin core, Supporting Information). The nomenclature $a\_b$ indicates that orbital $a$ interacts with $b$ and that $a$ has a larger contribution to the resulting MO.

show ground states where the $d_{xy}$ orbital is at lower energy.[44] But known exceptions of low-spin iron(III) systems where $d_{xy}$ is at higher energy have $\pi$-accepting axial ligands such as weakly basic pyridines[45,46] or isocyanides[47] demonstrating the importance of axial ligation.

The difference in the d orbital energy sequence between iron(II) and iron(III) can be rationalized as follows. First, in the ferric oxidation state, the d orbitals are at low energy, and correspondingly, the porphyrin serves mostly as a $\pi$ donor ligand. This $\pi$ donation leads to an increase in the energy of the $d_{xz}$ and $d_{yz}$ orbitals relative to $d_{xy}$. On the other hand, in the ferrous oxidation state, the d orbitals are at high energy, and correspondingly, the porphyrin now serves as a backbonding ligand. This interaction lowers the energy of the $d_{xz}$ and $d_{yz}$ orbitals relative to $d_{xy}$. Because of the general nature of this effect, we believe that the electronic structure description elaborated for [Fe(TPP)(2-MeHIm)] is in general representative for class **N** high-spin ferrous porphyrin complexes.

In contrast, the electronic structure of class **A** complexes shows significant differences. Figure 10 shows the frontier

(44) Walker, F. A. *Chem. Rev.* **2004**, *104*, 589.
(45) Safo, M. K.; Gupta, G. P.; Watson, C. T.; Simonis, U.; Walker, F. A.; Scheidt, W. R. *J. Am. Chem. Soc.* **1992**, *114*, 7066.
(46) Safo, M. K.; Walker, F. A.; Raitsimring, A. M.; Walters, W. P.; Dolata, D. P.; Debrunner, P. G.; Scheidt, W. R. *J. Am. Chem. Soc.* **1994**, *116*, 7760.
(47) Walker, F. A.; Nasri, H.; Turowska-Tyrk, I.; Mohanrao, K.; Watson, C. T.; Shokhirev, N. V.; Debrunner, P. G.; Scheidt, W. R. *J. Am. Chem. Soc.* **1996**, *118*, 12109.

**Figure 10.** Frontier $\beta$-MO diagram of [Fe(TPP)(2-MeIm$^-$)]$^-$ calculated with BP86/TZVP. The applied coordinate system is chosen such that $x$ and $y$ are located in the porphyrin plane, and $z$ is orthogonal to the porphyrin ring in the direction of the axial ligand. $E_{(g)}$ refers to the LUMO of the porphyrin as shown in Figure S4 (the index g is put in brackets because of the low symmetry of the porphyrin core, Supporting Information). The nomenclature $a\_b$ indicates that orbital $a$ interacts with $b$ and that $a$ has a larger contribution to the resulting MO.
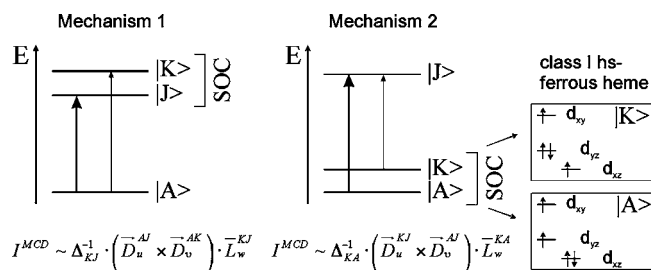
region of the $\beta$-MO diagram of [Fe(TPP)(2-MeIm$^-$)]$^-$, obtained for the observed solid-state structure with BP86/TZVP. In this case, the single $\beta$-d electron occupies an MO that corresponds to $d'_{xy}$ with a small admixture of $d_{xz}$. This mixing leads to a rotation of the $d_{xy}$ orbital out of the $xy$ plane. A contour plot of the $t_2$ type orbital obtained this way is shown in Figure 10. As evident from the contour plot, this rotation of the $d'_{xy}$ orbital enables a $\sigma$ backbond with one component of the $E_{(g)}$ LUMO of the porphyrin. Note that the label $d'_{xy}$ is used in the following to indicate that this orbital actually corresponds to a combination of the $d_{xy}$ and $d_{x^2-y^2}$ orbitals ($\sim$3:1 ratio), which leads to a slight rotation of the $d_{xy}$ orbital in the $xy$ plane to optimize bonding in the distorted symmetry of the complex. A second combination of $d'_{xy}$ and the porphyrin $E_{(g)}$ LUMO is observed only 1365 cm$^{-1}$ higher in energy than the occupied $\beta$-d MO as shown in Figure 10. In summary, the $d'_{xy}$ orbital is observed at lowest energy in [Fe(TPP)(2-MeIm$^-$)]$^-$, which is strikingly different from [Fe-(TPP)(2-MeHIm)]. This relates to the very large out-of-plane displacement of iron in [Fe(TPP)(2-MeIm$^-$)]$^-$, which allows for the $d'_{xy}$ orbital to undergo a backbonding interaction with the $E_{(g)}$ LUMO of the porphyrin as illustrated by the contour plot of the $d'_{xy}/d_{xz}-E_{(g)}$ MO in Figure 10. In contrast, $d_{xy}$ is strictly nonbonding in the case of [Fe(TPP)(2-MeHIm)]. Finally, the $d_{xz}$ and $d_{yz}$ orbitals are observed at highest energy in the case of [Fe(TPP)(2-MeIm$^-$)]$^-$, which is due to the fact that imidazolate is a distinctly stronger donor than imidazole. This affects in particular $d_{yz}$, which interacts with an occupied $\pi$ orbital of imidazolate, as evident from the contour plot in Figure 10. This shifts the $d_{yz}$ orbital to unusually high energy. In contrast, $d_{xz}$

**Figure 11.** MCD **C**-term mechanisms (left, middle), and example for mechanism 2 for class **N** five-coordinate high-spin ferrous heme complexes like [Fe(TPP)(2-MeHIm)] (right).

mixes with an imidazolate (in-plane) $\sigma$ orbital, which is a weaker interaction, causing the energy splitting between $d_{xz}$ and $d_{yz}$ ('rhombicity'). The principal electronic structure descriptions do not change when the fully optimized structures of these compounds are considered, as evident from Figures S5−S7 (Supporting Information).

With the electronic structure descriptions of [Fe(TPP)(2-MeHIm)] and [Fe(TPP)(2-MeIm$^-$)]$^-$ clearly laid out, an interesting question is how the properties of class **A** complexes change if the anionic axial ligand is an isotropic $\pi$ donor, such that $d_{xz}$ and $d_{yz}$ experience the same level of energetic destabilization. In order to evaluate this case, we consider the chloride complex [Fe(TPP)Cl]$^-$. Figure S7 (Supporting Information) shows the $\beta$-MO diagram for this complex in the frontier region, which strikingly supports our previous analysis. In this case, the $\beta$-d electron again occupies an orbital that has predominant $d_{xy}$ character (50% $d_{xy}$ plus 11% $d_{xz}$ as shown in Figure S7, Supporting Information). Both the $d_{xz}$ and $d_{yz}$ orbitals are now high in energy, due to chloride having equivalent $3p_x$ and $3p_y$ donor orbitals. This supports the previous conclusion that $d_{yz}$ in [Fe(TPP)(2-MeIm$^-$)]$^-$ is high in energy because of imidazolate being a strong $\pi$ donor.

On the basis of these results, the two important general differences between the electronic structures of class **N** and class **A** five-coordinate high-spin ferrous heme complexes are: (a) $d_{xy}$ is low in energy in class **A** compounds due to the large out-of-plane displacement of iron, which allows for a backbonding interaction with the porphyrin $E_{(g)}$ LUMO, and (b) $d_{yz}$ and $d_{xz}$ are high in energy due to the presence of strong anionic ($\pi$) donor ligands. As a consequence, the $\beta$-d electron occupies the $d_{xz}$ orbital in class **N** compounds, and the $d_{xy}$ orbital in class **A** complexes. This difference in electronic structure is directly reflected by the molar MCD intensities of these complexes, as further evaluated below.

**Electronic Structure and MCD Intensity.** With the electronic structure descriptions of all three complexes in hand, we can now analyze the observed drastic difference in low-temperature MCD intensities between these complexes. In general, MCD **C**-term intensity is due to two different mechanisms, which require spin−orbit coupling between two energetically close excited states (mechanism 1), or the ground state and a low-lying excited state (mechanism 2). Figure 11 shows illustrations of these mechanisms, together with mathematical expressions for the resulting MCD **C**-term intensities as derived in ref 48. Here, $\bar{D}_u^{AJ}$ is the transition dipole moment for the electronic transition between states $|A\rangle$ and $|J\rangle$ in direction $u$ ($u, v, w = x, y, z$), $\Delta_{KJ}^{-1}$ is the energy difference between states $|K\rangle$ and $|J\rangle$, and $\bar{L}_w^{KJ}$ is the reduced SOC matrix element between states $|K\rangle$

(48) Neese, F.; Solomon, E. I. *Inorg. Chem.* **1999**, *38*, 1847.

and $|J\rangle$ in direction $w$. These equations show that **C**-term intensity requires two orthogonal electric dipole allowed transitions, where either the excited states (mechanism 1) or the ground and a low-lying excited state (mechanism 2) are spin−orbit coupled in a direction orthogonal to the plane formed by the two transition dipole moments. Previous work of one of us has shown that for the Soret, Q, and Q$_v$ bands, mechanism 1 leads to a pseudo-**A** (derivative-shaped) **C**-term signal in the MCD spectrum.[38] This is due to the fact that metalloporphyrins do not show strict 4-fold symmetry, leading to a small energy splitting between the two components of the $E_{(g)}$ LUMO of the porphyrin. Since the Soret, Q, and Q$_v$ bands are mostly in-plane ($x$, $y$) polarized, the corresponding excited states can then spin−orbit couple in the $z$ direction ($w = z$ in mechanism 1). Besides this, mechanism 2 becomes important when low-lying (ligand field) excited states are available, for example in the case of low-spin ferric porphyrins. As one of us has shown recently, the two different electron configurations $[d_{xy}]^2 [d_{xz}, d_{yz}]^3$ (unpaired electron located in the $d_{xz}$ or $d_{yz}$ orbital) and $[d_{xz}, d_{yz}]^4 [d_{xy}]^1$ (unpaired electron located in $d_{xy}$) differ significantly with respect to SOC in $z$ direction, and hence, can be distinguished using low-temperature MCD spectroscopy (see Discussion in ref 40). In a similar fashion, the MCD intensity differences between all three complexes investigated here relate to mechanism 2, that is, changes in the $t_2$-type $\beta$-d orbitals. Indeed, as described above, all three compounds differ quite strongly in the properties of these orbitals. In the following, we will use the observed Soret band MCD intensity to compare the properties of all complexes.

Assuming that state $|K\rangle$ in mechanism 2 is a low-lying ligand field excited state, and keeping in mind that the Soret band is $x$, $y$ polarized, the **C**-term intensity for this feature is predominantly generated by SOC in the $z$ direction. The corresponding reduced SOC matrix element between the ground state $|A\rangle$ and the low-lying excited state $|K\rangle$ is defined as (cf. mechanism 2 in Figure 11):

$$\bar{L}_z^{KA} = \text{Im}\langle K|\mathbf{H}_{SOC}^z|A\rangle \qquad (1)$$

where $\mathbf{H}_{SOC}^z = \Sigma_A \xi(r_A)l_{A,z}$ (the integrals over the spin functions have already been taken into account in the derivation).[48] Here, the sum runs over all atoms $A$ of the molecule, $\xi(r_A)$ is the radial SOC operator of atom $A$, and $l_{A,z}$ is the angular momentum operator $l_z$ on center $A$. Using the LCAO approximation for molecular orbitals, that is, $|K\rangle = \Sigma_r c_r \phi_r$ and $|A\rangle = \Sigma_s c_s \phi_s$, and neglecting two- and three-center integrals, the total SOC contribution becomes:

$$\frac{\text{Im}\langle K|\mathbf{H}_{SOC}^z|A\rangle}{\Delta_{KA}} = \frac{\text{Im}[\sum_A \zeta^A \sum_{r,s} \langle c_r \phi_r^A | l_{A,z} | c_s \phi_s^A \rangle]}{\Delta_{KA}} \qquad (2)$$

where $\zeta^A$ is the one-electron spin−orbit coupling constant of atom $A$. Importantly, the value of this integral is dominated by the contributions of iron d orbitals for two reasons: (a) the SOC constant $\zeta_{3d}$ for iron(II) is about 400 cm$^{-1}$,[48] which is much larger than SOC constants for light elements like C and N, and (b) since $l_{A,z}|p_z^A\rangle = 0$, the integrals in eq 2 should all vanish for pure porphyrin $\pi$ or $\pi^*$ MOs. Although the d orbitals in the complexes all show quite large admixtures of the porphyrin $E_{(g)}$ LUMO $\pi^*$ orbitals (vide supra), these contributions can therefore be neglected for the SOC matrix elements in eq 2, which become:

$$\frac{Im[\sum_A \zeta^A \sum_{r,s} \langle c_r \phi_r^A | l_{A,z} | c_s \phi_s^A \rangle]}{\Delta_{KA}} = \frac{Im[\zeta^{Fe} \sum_{r,s} \langle c_r^d \phi_r^d | l_z | c_s^d \phi_s^d \rangle]}{\Delta_{KA}}$$

(3)

where the $\phi^d$ now refer to the principal d orbitals of iron. Equation 3 can be used to obtain qualitative insight into the relative MCD C-term intensities for the three complexes of interest. A quantitative evaluation is prohibited by the fact that the intensity contribution from mechanism 1 is not exactly known, but should at least be quite similar for the three complexes of interest.

For [Fe(TPP)(2-MeHIm)], the four lowest lying excited states (using the nomenclature from Figure 9) give rise to the four contributions:

$$Im[\zeta^{Fe}\langle d_{yz}\_E_{(g)} | l_z | d_{xz}\_E_{(g)} \rangle] \quad Im[\zeta^{Fe}\langle d_{xy} | l_z | d_{xz}\_E_{(g)} \rangle] = 0$$
$$Im[\zeta^{Fe}\langle E_{(g)}\_d_{xz} | l_z | d_{xz}\_E_{(g)} \rangle] = 0 \quad Im[\zeta^{Fe}\langle E_{(g)}\_d_{yz} | l_z | d_{xz}\_E_{(g)} \rangle]$$

Since SOC has to be active in the z direction, the matrix elements $\langle d_{xy} | l_z | d_{xz} \rangle$ and $\langle d_{xz} | l_z | d_{xz} \rangle$ vanish. *Importantly, this means that $d_{xy}$ cannot contribute to MCD intensity for x, y polarized transitions.* In addition, $Im\langle d_{yz} | l_z | d_{xz} \rangle = 1$.[49] Using the ground state molecular orbital coefficients, and the orbital energies as a rough approximation for the corresponding excited state energies from Figure 9, one can estimate that the contribution from $\langle d_{yz}\_E_{(g)} | l_z | d_{xz}\_E_{(g)} \rangle$ will be dominating. (From TD-DFT: $d_{yz}\_E_{(g)}$ excited state = +1543 cm$^{-1}$.) The same type of analysis can be applied to [Fe(TPP)(2-MeIm$^-$)]$^-$, which allows us to approximate the C-term intensity ratio between complexes [Fe(TPP)(2-MeHIm)] and [Fe(TPP)(2-MeIm$^-$)]$^-$. In the case of [Fe(TPP)(2-MeIm$^-$)]$^-$, the dominating contribution to MCD intensity comes from the integral $\langle d_{yz}\_E_{(g)} | l_z | d'_{xy}/d_{xz}\_E_{(g)} \rangle$. (From TD-DFT: $d_{yz}\_E_{(g)}$ excited state = +5741 cm$^{-1}$.) Considering the main d-orbitals of complexes [Fe(TPP)(2-MeHIm)] and [Fe(TPP)(2-MeIm$^-$)]$^-$, the MCD C-term ratio between complexes [Fe(TPP)(2-MeHIm)] and [Fe(TPP)(2-MeIm$^-$)]$^-$ is roughly estimated to be ~6:1. (Using TD-DFT excited state energies, the ratio becomes 7:1.) This number is somewhat low compared to experiment, which could be due to the fact that (a) the orbital energies are only crude approximations of the corresponding excited state energies, and more importantly, (b) the occupied $\beta$-d orbital of [Fe(TPP)(2-MeIm$^-$)]$^-$ still shows a distinct $d_{xz}$ admixture, which might not be the case experimentally.

## Discussion

This study began with the idea that there are at least two distinctly different electronic states of high-spin iron(II) porphyrinates. This dichotomy was initially seen from the clear structural differences between five-coordinate species with a neutral nitrogen donor versus species with an anionic axial ligand. These differences are schematically depicted in Figure 2 for the iron(II) derivatives with imidazole and imidazol*ate* as the axial ligand. The values shown for imidazolate are the averages for the structures reported earlier[12] and those for the imidazole averages are drawn from previously defined structures.[10,11,13–15] Although both types of species are high-spin (S = 2), the coordination geometry differences are striking. As

can be seen in Figure 2, the iron displacement from the four nitrogen atom plane and the Fe–N$_p$ bond distances are both significantly larger in the imidazolate than in the imidazole derivatives. Simply put, in the imidazolate derivatives the size of the iron(II) atom appears to be larger than it is in the imidazole species. The structures for a number of iron(II) species with an axial anionic ligand are similar to those of the imidazolate derivatives as well as that of anionic [Fe(TPP)Cl]$^-$ reported herein. The strong similarities between members of each group strongly suggested that the origin of these structural differences are the consequence of differing electronic structures.

In exploring this possible dichotomy in this paper, we distinguish between two classes of iron(II) porphyrinate derivatives, which we call Class **N**, those species with neutral, mostly nitrogen donors, and Class **A**, those species with an anionic axial ligand. Clearly, the charge on the axial ligand has a strong effect on the electronic structure. Because the d-orbitals are all at relatively high energy in the ferrous state, the $\pi$-donating character of the anionic ligands leads to the raising of the $d_{xz}$ and $d_{yz}$ orbital energies and concomitant relative lowering of the energy of the $d_{xy}$ orbital which then becomes the doubly occupied orbital. This effect holds whether the axial ligand has two equivalent $\pi$-donor orbitals ($p_x$ and $p_y$), as in the case of atomic anions (halides, oxyanions), or anisotropic (in-plane and out-of-plane) $\pi$ donor orbitals, as in the case of imidazolate, hydroxide, or thiolate ligands. Keeping in mind that protonation/deprotonation in the imidazole case occurs at the distant $\varepsilon$-N atom, formally $sp^2$ hybridized, the strong effect of the protonation state of this N-atom on the electronic structure of the complex is certainly surprising. In contrast, the corresponding change in electronic structures in the cases of water versus hydroxide, or thiol versus thiolate complexes is somewhat less surprising, since in these cases the deprotonation occurs directly at the coordinating donor atom, thereby strongly increasing its $\pi$-donor abilities. This increase in $\pi$ donation also strengthens the Fe—(anionic ligand) bonds as evident from the shorter Fe–N bond distance in imidazolate versus imidazole complexes. This basis for the electronic structure differences suggests that a five-coordinate aqua species would be a class **N** whereas a hydroxo species would be class **A**. Indeed, de Gracia et al.[50] describe solution-based Raman and UV–vis spectroscopy for five-coordinate high-spin ferrous aqua and hydroxo complexes, which they conclude have the same electronic structures as the analogous imidazole and imidazolate species, respectively. We believe that these class **N** and **A** groupings are broadly applicable and we expect additional data will continue and strengthen the classification. Classification of six-coordinate high-spin ferrous species is somewhat limited. We note that the only well-characterized six-coordinate high-spin iron(II) species are those of bis(tetrahydrofuran) coordination[51,52] that are clearly shown to be members of class **N** by Mössbauer characterization.[51]

As we have outlined in Results and Analysis, we have explored several physical approaches to determine whether the methods provide clear-cut distinctions between the two classes of high-spin iron(II) porphyrinates. In every case, within the

(49) Lever, A. B. P.; Solomon, E. I. Ligand Field Theory and the Properties of Transition Metal Complexes. In *Inorganic Electronic Structure and Spectroscopy*, Volume 1; Solomon, E. I., Lever, A. B. P., Eds.; Wiley: New York, 1997.

(50) de Gracia, A. G.; Bordes, L.; Desbois, A. *J. Am. Chem. Soc.* **2005**, *127*, 17634.

(51) Reed, C. A.; Mashiko, T.; Scheidt, W. R.; Spartalian, K.; Lang, G. *J. Am. Chem. Soc.* **1980**, *102*, 2302.

(52) Hu, C.; Noll, B. C.; Scheidt, W. R. *Acta Crystallogr., Sect. E* **2005**, *61*, m830–m831.

(53) The best choice of mean plane comparison is the displacement of iron from the mean plane of the central four nitrogen atoms as this minimizes effects from differing core conformations.

necessary limitations of a small number of examples, the result is in the affirmative, and we briefly summarize the strengths and limitations of each approach.

**I. X-ray Analysis.** Assigning electronic states from the molecular structure of course requires obtaining an X-ray quality crystal and getting a reasonably precise and accurate structure. With those requirements accomplished, the results needed for assignment to the two classes are fairly unambiguous, based on the coordination group parameters and especially the values of Fe−N$_p$ and the displacement of the iron from the mean planes.[53] To our knowledge, only the group of high-spin thiolate-ligated hemes have structural parameters intermediate to those of class **N** and class **A**. Cataloguing their behavior with other physical methods is still not complete, but their position as members of class **A** seems certain based on the available Mössbauer data.[21] Finally and unfortunately, the X-ray method is not easily applicable to the assignment of the electronic structure of the heme centers of proteins.

**II. Mössbauer Spectroscopy.** The measurement and fitting of Mössbauer spectra obtained in high field leads to the unequivocal assignment of the sign of $\Delta E_q$. The sign of $\Delta E_q$ for all members of class **N** is negative, whereas for all members of class **A** it is positive. For small molecule systems, obtaining enough material for an adequate signal-to-noise ratio is relatively straightforward but may present problems for some heme protein samples. The need for obtaining Mössbauer spectra in high applied magnetic field (and concomitant low temperature) in order to unequivocally determine the sign of the quadrupole splitting constant and somewhat larger sample sizes are the major limitation for the use of this method. The use of $^{57}$Fe -labeled proteins would clearly aid in making good measurements on proteins.

**III. EPR Spectroscopy.** As described earlier the integer-spin EPR spectra clearly show that the class **N** examples have a positive sign for *D*, whereas those for class **A** have a negative value of *D*. Establishing the experimental requirements for integer-spin EPR spectra can be challenging, but the major limitation is the magnitude of *D*, which if too large will render a sample EPR silent. Although it seems that most samples are within the values needed for the X-band range, measurements at higher frequencies can alleviate this issue. As is well-known, the sensitivity of EPR spectroscopy means that relatively small samples of a heme protein are required for good measurements.

**IV. MCD Spectroscopy.** The difference in the electronic structures of class **N** and class **A** high-spin ferrous hemes is clearly reflected by the absolute molar **C**-term intensities of the signals, as demonstrated here for the first time. Note that MCD also distinguishes between high-spin and low-spin ferric porphyrins in a similar way.[40] For practical purposes, comparison of the **C**-term intensities of the very intense Soret bands is best, which also allows for the usage of quite dilute samples (<100 $\mu$M). On the other hand, the observed energies of the transitions, and the overall appearance of the spectra do not show much variation in the case of high-spin ferrous hemes, and hence, cannot be used to distinguish between the two classes. The advantage of MCD spectroscopy is the small amount of sample needed in order to determine the **C**-term intensity of the Soret band. With sample volumes in the range of 2−3 mL, the total amount of protein required is <0.2 $\mu$mol. For the measurement, frozen glasses are needed, which are usually easily achieved for proteins by addition of glycerol. Finding a combination of organic, noncoordinating solvents that glass upon freezing for the small molecule studies is a bigger challenge, and sometimes

several attempts are needed to obtain a glass of sufficient quality for measurement.

**V. DFT Approaches.** DFT calculations on the BP86/TZVP level are able to provide good ground state descriptions that are in overall agreement with experiment if based on known experimental structures. As shown in this paper, and as noticed before,[54,40] DFT is challenged when it comes to the prediction of the correct out-of-plane distortion of the porphyrin ring, which affects the accuracy of ground state property (EPR, zero-field splitting, and Mössbauer parameters) predictions. Hence, when only DFT-optimized structures are used, the confidence level of the DFT results is lower. The properties that show the least amount of variation between the experimental and optimized structures are (a) the nature of the MO that carries the single $\beta$-electron, and (b) the calculated sign of the Mössbauer quadrupole tensor. These two properties show good agreement with experiment even if the somewhat flawed DFT structures are used for the calculations. Hence, high-level DFT calculations can significantly help predict ground states for high-spin ferrous hemes in new complexes or proteins, particularly when correlated with spectroscopic studies.

The initial recognition of two possible types of high-spin iron(II) electronic structures led to this multimethod study to examine various possible experimental methods for discrimination. We have outlined several methods that we show can be used successfully to make distinctions between the two classes of high-spin d$^6$ porphyrinates. The two classes are distinguished by the difference in character of the one doubly occupied d orbital. Although there may be some minor differences within each class, in the class **N** complexes the doubly occupied orbital is effectively perpendicular to the porphyrin plane. Moreover, this orbital is in the plane of the ligated imidazole as shown by the DFT calculations reported herein (d$_{xz}$ in the coordinate system applied here). In class **A** species, on the other hand, the doubly occupied orbital has principally d$_{xy}$ character. Some variation occurs as the $\pi$ bonding character of the axial ligand changes and there is some symmetry lowering in imidazolate vs chloride, but the doubly occupied orbital can be considered effectively parallel to the heme plane. We emphasize that we believe that the distinction of the two groups of high-spin iron(II) porphyrinates is generally applicable to all high-spin iron(II) systems.[55]

Does this recognition of electronic state differences provide new insight into the oft-asked question of the role of the proximal ligand in heme proteins? We believe so. The differences must clearly reflect differences in the function of the heme protein; a tenet of many bioinorganic metalloprotein studies is that electronic structure contributes to function. This clearly is seen in the proteins that can be definitively assigned to one of the two classes. Deoxyhemoglobin and -myoglobin, members of class **N**, are reversible O$_2$ binders. The O$_2$ complex has (partial) ferric-superoxide character;[56] the location of the single $\beta$-electron in a t$_{2g}$-type orbital that is orthogonal to the heme-plane and overlaps with the incoming O$_2$ is certainly advantageous for O$_2$ binding and electron transfer. In addition, imidazole is a weaker ligand than imidazolate, which helps to stabilize

(54) Lehnert, N.; Silvernail, N. J.; Sage, J. T.; Scheidt, W. R.; Sturhahn, W.; Zhao, J. ms. in preparation.

(55) We note that the one known group of six-coordinate high-spin iron(II) species are those with two neutral tetrahydrofuran ligands.[51,52] Mössbauer characterization clearly places these in the class **N** group.[51]

(56) (a) Weiss, J. J. *Nature* **1964**, *203*, 183. (b) Reed, C. A.; Momenteau, M. M. *Chem. Rev.* **1994**, *94*, 659.

the O$_2$ complex by avoiding a $\sigma$-trans interaction between the axial ligands. In this sense, the Fe−N(His) bond strength could be used to fine-tune the properties of the Fe−O$_2$ bond, and this could be mediated by the strength of the hydrogen bond to the His imidazole ring. This is yet another indication of how well fine-tuned the active sites of Hb and Mb are for O$_2$ binding and transport. On the other hand, HRP and potentially cytochrome P450, members of class **A**, are involved in catalytic oxidations and do not reversibly bind O$_2$. In this case, the link to function is likely due to the fact that stronger donating, anionic proximal ligands promote heterolytic O−O bond cleavage, leading to formation of high-valent ferryl intermediates. This has to be avoided in Mb and Hb, so in these cases, the weaker imidazole donor is preferred over imidazolate as in HRP.

Thus to the extent that data are currently available for proteins, they also follow the classification. Now that the possible significance of electronic state differences are known, we expect that further heme protein classification will be made. Currently the best data are from Mössbauer, but as noted in this paper, MCD may become the most generally useful method for categorizing. From the class **N** and **A** classification from spectroscopy it might therefore be possible to predict the likely function of a newly discovered heme protein, i.e. whether it might serve as O$_2$ binder or sensor, or as an O$_2$ activating peroxidase, hydroxylase, etc.

Another interpretation of the biological importance of the electronic structure differences has been provided by theoretical investigations of Jensen and Ryde, who have studied the effects of hydrogen bonding to imidazole on the properties of histidine-ligated heme proteins.[57] They have noted that hydrogen bonding leads to large changes in the relative energies of the high-spin state and the intermediate-spin state. In the presence of weak, or no, hydrogen bonding, the ferrous state shows very small differences between the two spin states. Indeed, the difficulty of predicting the correct ground state for deoxymyoglobin models is demonstrated by the number of DFT calculations that failed to correctly predict the high-spin ground state.[58] Jensen and Ryde also showed that in the presence of strong hydrogen bonding to histidine, it is conversely the ferric state that shows

the small difference between the intermediate- and high-spin states.[57] They further suggest that it is this difference that leads to the differences in function. In a subsequent paper,[59] they suggest that the closeness of varying spin states in the deoxy-derivatives is essential for facile O$_2$ binding and that this is the solution to the spin-forbidden nature of the reaction and to the differing nature of HRP. We do note, however, that Jensen and Ryde did not suggest differences in the ground state descriptions for the different hydrogen-bonded states, which may simply be a reflection of the difficulty of the calculations.

Where else might the issue of the two electronic states in iron(II) be of biological significance? Although we are unaware of any definitive data on the issue, we suspect that proteins like the gas-sensing heme proteins, such as FixL or soluble guanyl cyclase, will found to be members of class **N** whereas heme proteins involved in O$_2$ activation will be found to be members of class **A**. The differences between the class **N** and **A** species are not simply the strength of the ligand field. Although it is known that imidazole is a weaker field ligand that imidazolate,[60] imidazole is clearly a stronger field ligand than chloride, a class **A** ligand like imidazolate. Thus, the distinction is not simply a ligand field parameter. Further developments in the significance of this dichotomy will wait characterization of more heme proteins in one or the other cases.

**Supporting Information Available:** Figures S1−S3, comparing DFT-calculated and observed structural parameters for [Fe(TPP)(2-MeHIm)]$^-$, [Fe(TPP)(2-MeIm$^-$)]$^-$, and [Fe-(TPP)Cl]$^-$; Figure S4, MO diagram for free porphine; Figures S5−S7 giving MO diagrams for the fully optimized structures of [Fe(TPP)(2-MeHIm)]$^-$, [Fe(TPP)(2-MeIm$^-$)]$^-$, and [Fe-(TPP)Cl]$^-$; details of the structure determination for K(222)-[Fe(TPP)Cl], complete ref 27; Tables S1−S6 giving complete details for the structure of K(222)[Fe(TPP)Cl]. Crystallographic data is available as a CIF file. This material is available free of charge via the Internet at http://pubs.acs.org.

(57) Jensen, K. P.; Ryde, U. *Mol. Phys.* **2003**, *101*, 2003.
(58) (a) Rovira, C.; Kunc, K.; Hutter, J.; Ballone, P.; Parrinello, M. *J. Phys. Chem. A* **1997**, *101*, 8914. (b) Kozlowski, P. M.; Spiro, T. G.; Zgierski, M. Z. *J. Phys. Chem. B* **2000**, *104*, 10659. (c) Ugalde, J. M.; Dunietz, B.; Dreuw, A.; Head-Gordon, M.; Boyd, R. J. *J. Phys. Chem. A* **2004**, *108*, 4653.

(59) Jensen, K. P.; Ryde, U. *J. Biol. Chem.* **2004**, *279*, 14561.
(60) Landrum, J. T.; Hatano, K.; Scheidt, W. R.; Reed, C. A. *J. Am. Chem. Soc.* **1980**, *102*, 6729.